



HAL
open science

Petrogenesis of LREE-rich pegmatitic granite dykes in the central Grenville Province by partial melting of Paleoproterozoic-Archean metasedimentary rocks: Evidence from zircon U-Pb-Hf-O isotope and trace element analyses

François Turlin, Olivier Vanderhaeghe, Félix Gervais, Anne-Sylvie André-Mayer, Abdelali Moukhsil, Armin Zeh, Fabien Solgadi, Iptn Iptn

► To cite this version:

François Turlin, Olivier Vanderhaeghe, Félix Gervais, Anne-Sylvie André-Mayer, Abdelali Moukhsil, et al. Petrogenesis of LREE-rich pegmatitic granite dykes in the central Grenville Province by partial melting of Paleoproterozoic-Archean metasedimentary rocks: Evidence from zircon U-Pb-Hf-O isotope and trace element analyses. *Precambrian Research*, 2019, 327, pp.327-360. 10.1016/j.precamres.2019.02.009 . hal-02166886

HAL Id: hal-02166886

<https://hal.univ-lorraine.fr/hal-02166886>

Submitted on 27 Jun 2019

HAL is a multi-disciplinary open access archive for the deposit and dissemination of scientific research documents, whether they are published or not. The documents may come from teaching and research institutions in France or abroad, or from public or private research centers.

L'archive ouverte pluridisciplinaire **HAL**, est destinée au dépôt et à la diffusion de documents scientifiques de niveau recherche, publiés ou non, émanant des établissements d'enseignement et de recherche français ou étrangers, des laboratoires publics ou privés.



Distributed under a Creative Commons Attribution - NonCommercial - NoDerivatives 4.0 International License

Accepted Manuscript

Petrogenesis of LREE-rich pegmatitic granite dykes in the central Grenville Province by partial melting of Paleoproterozoic-Archean metasedimentary rocks: evidence from zircon U-Pb-Hf-O isotope and trace element analyses

François Turlin, Olivier Vanderhaeghe, Félix Gervais, Anne-Sylvie André-Mayer, Abdelali Moukhsil, Armin Zeh, Fabien Solgadi, I.P.T.N.

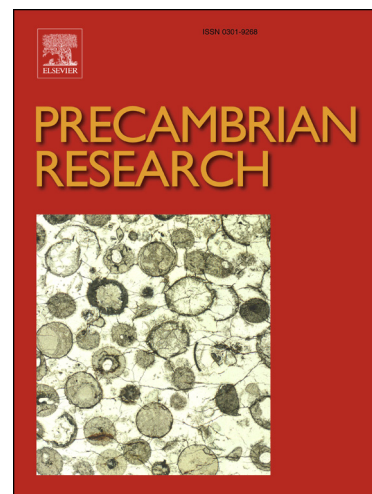
PII: S0301-9268(18)30492-3
DOI: <https://doi.org/10.1016/j.precamres.2019.02.009>
Reference: PRECAM 5284

To appear in: *Precambrian Research*

Received Date: 24 September 2018
Revised Date: 1 February 2019
Accepted Date: 12 February 2019

Please cite this article as: F. Turlin, O. Vanderhaeghe, F. Gervais, A-S. André-Mayer, A. Moukhsil, A. Zeh, F. Solgadi, I.P.T.N., Petrogenesis of LREE-rich pegmatitic granite dykes in the central Grenville Province by partial melting of Paleoproterozoic-Archean metasedimentary rocks: evidence from zircon U-Pb-Hf-O isotope and trace element analyses, *Precambrian Research* (2019), doi: <https://doi.org/10.1016/j.precamres.2019.02.009>

This is a PDF file of an unedited manuscript that has been accepted for publication. As a service to our customers we are providing this early version of the manuscript. The manuscript will undergo copyediting, typesetting, and review of the resulting proof before it is published in its final form. Please note that during the production process errors may be discovered which could affect the content, and all legal disclaimers that apply to the journal pertain.



Petrogenesis of LREE-rich pegmatitic granite dykes in the central Grenville Province by partial melting of Paleoproterozoic-Archean metasedimentary rocks: evidence from zircon U-Pb-Hf-O isotope and trace element analyses

François Turlin^{a,b,*}, Olivier Vanderhaeghe^c, Félix Gervais^d, Anne-Sylvie André-Mayer^a, Abdelali Moukhsil^e, Armin Zeh^f, Fabien Solgadi^g, I.P.T.N.^h

^a *GeoRessources lab., Université de Lorraine, CNRS, CREGU, Campus Aiguillettes, Faculté des Sciences et Technologies, rue Jacques Callot, Vandœuvre-lès-Nancy, F-54506, France*

^b *Now at Université du Québec à Montréal, Département des Sciences de la Terre et de l'Atmosphère, 201, ave. du Président-Kennedy, Montréal, QC, Canada H2X 3Y7*

^c *Géosciences Environnement Toulouse, UMR 5563, GET, Université de Toulouse, UPS, CNRS, IRD, CNES, France*

^d *Département des génies civil, géologiques et des mines, Polytechnique Montréal, Canada*

^e *Ministère de l'Énergie et des Ressources naturelles, Direction du Bureau de la connaissance géoscientifique du Québec, 5700, 4e Avenue Ouest, Québec (Québec), G1H 6R1*

^f *KIT-Karlsruhe Institute of Technology, Campus South, Institute for Applied Geosciences, Mineralogy and Petrology, Adenauerring 20b, Geb. 50.40, 76131 Karlsruhe*

^g *Ministère de l'Énergie et des Ressources naturelles, Direction du Bureau de la connaissance géoscientifique du Québec, 400, boulevard Lamaque, Val-d'Or (Québec) J9P 3L4*

^h *Ion Probe Team Nancy, CRPG, UMR 7358, CNRS, Université de Lorraine, Vandœuvre-lès-Nancy, F-54501, France*

* Corresponding author at: François Turlin

Université du Québec à Montréal

Département des sciences de la Terre et de l'atmosphère

201, avenue du Président-Kennedy

Montréal, Québec, H2X 3Y7

Mail: turlin.francois@courrier.uqam.ca

ACCEPTED MANUSCRIPT

Abstract

The Allochthonous Belt of the central Grenville Province in Quebec (Canada) hosts LREE-rich pegmatitic granite dykes (PGDs) intrusive into orthogneisses and migmatitic paragneisses. Zircon crystals from a monazite-bearing PGD and two allanite-bearing PGDs of the Lac Okaopéo region were investigated. Concordia U-Pb ages of 1004.2 ± 2.1 Ma, 1001.9 ± 3.9 Ma and 1004.2 ± 2.3 Ma, respectively, indicate that emplacement of the dykes occurred during the early-Rigolet orogenic phase. Trace element contents (U, Yb, Y) of zircon grains, their subchondritic $\varepsilon_{\text{Hf}}(1003 \text{ Ma})$ values from -4.7 to -11.8, Hf model ages from 2.05 to 2.44 Ga, and predominant supra-mantle $\delta^{18}\text{O}_{\text{V-SMOW}}$ values (>5.3 ‰) indicate that the dykes were formed by partial melting of Paleoproterozoic-Archean metasedimentary rocks equivalent to those exposed in the Parautochthonous Belt (Knob Lake Group paragneisses), and located beneath the thickened Allochthonous Belt. This implies that the Parautochthonous Belt is present beneath the Allochthonous Belt hosting the LREE-rich PGDs and that it was affected by horizontal ductile flow towards the north for at least 80 km where it is currently exhumed along the Grenville Front.

Keywords: Zircon; U-Pb-Hf-O isotopes; Trace element; Grenville Province; Pegmatitic granite; LREE mineralization

1. Introduction

Tracing the source(s) of igneous rocks and their petrogenesis in the frame of the tectonometamorphic evolution of the crust is a recurrent theme in geology, especially for granitic magmas for which most of the debate focuses on the relative importance of mantle vs crustal input and the differing evolutions of collision- and subduction-related magmatism (Barbarin, 1999; Chappell and White, 2001; de Sigoyer et al., 2014; Moyen et al., 2017; Pearce et al., 1984; Toé et al., 2013). When considering their pegmatitic end-members, studies have essentially focused on establishing their derivation by extreme fractionation of their igneous parentage, as shown by the commonly used classifications of Černý et al. (2012) and Černý and Ercit (2005) that distinguish their igneous parents on the basis of their orogenic (crustal shortening, subduction and collision: Li-Cs-Ta or LCT pegmatites) or anorogenic settings (crustal thinning and rifting: Nb-Y-F or NYF pegmatites) (Martin and De Vito, 2005, and references therein). However, several contributions have supported an origin of such rocks by partial melting of a crustal or of a mantle component, the latter associated with more or less crustal assimilation (e.g. Černý et al., 2012; Ercit, 2005; Lentz, 1991; London, 2016; Martin and De Vito, 2005; Müller et al., 2015). Pegmatitic granites are particularly abundant in the Grenville Province of Canada (e.g. Ayres and Černý, 1982; Ercit, 2005; Fowler and Doig, 1983; Groulier et al., 2018a; Masson and Gordon, 1981; Turlin et al., 2017). Lentz (1991) proposed a model of formation of Grenvillian REE-rich pegmatitic granite dykes (*further designated as 'PGD'*) by mid-crustal partial melting during exhumation of the root of the Grenvillian orogenic belt. However, this model is essentially based on the lack of coeval granitic plutons and should be confronted to data constraining the source of these magmas and their ages (Ercit, 2005; Lentz, 1991). The Grenville Province (Fig. 1) is considered as a large, hot, long-duration orogen (e.g. Rivers, 2008) with abundant evidence of partial melting (e.g. Indares et al., 2008; Jannin et al., 2018a; Slagstad et al., 2004; Timmermann et al., 2002; Turlin et al., 2018) and mafic

magmatism (Rivers and Corrigan, 2000). Accordingly, this province represents a potential target to test these hypotheses.

Turlin et al. (2017) reported the occurrence of LREE-rich (monazite-bearing or allanite-bearing) PGDs in the Lac Okaopéo region, located south of the Manicouagan Reservoir in the Allochthonous Belt of the central Grenville Province in Quebec (Canada, Figs. 2 and 3). The discordant contact of the PGDs relative to the structure of their host rocks, their magmatic textures, and U/Pb ages of monazite of ca. 1005-1000 Ma suggest a post-tectonic intrusion for the monazite-bearing PGD, at the transition between the Ottawa and Rigolet phases. Moreover, their peraluminous character points to partial melting of metapelitic rocks at depth, but the source(s) of the PGDs melts remain unconstrained. Metapelites are present at the base of the Allochthonous Belt and in the underlying Parautochthonous Belt and thus both could be implicated in the petrogenesis of these PGDs.

Over the last decades, zircon has proved to be one of the most reliable tools to place new constraints on both the timing of magmatic crystallization and the crust-mantle evolution by combining petrographical, geochemical, and Lu-Hf-O isotope analyses with U-Pb dating (e.g. Belousova et al., 2010; Cawood et al., 2013; Dhuime et al., 2012; Eglinger et al., 2017; Hawkesworth et al., 2009; Spencer et al., 2015; Zeh et al., 2014). In this study, we present trace element and U-Pb-Hf-O isotopic data of well characterized zircon grains from a monazite-bearing PGD and two allanite-bearing PGDs from the Lac Okaopéo region (central Grenville Province, Figs. 2 and 3). These data place new constraints on the nature of the PGD sources within the crust and mantle, and the timing of their intrusion. Furthermore, they provide new information about the deep-crustal processes which occurred during the Grenvillian Orogeny.

2. Geological framework

2.1. Geodynamic evolution of the central Grenville Province

The Grenville Province (Fig. 1a-b) resulted from protracted accretion along the southeastern margin of Laurentia from the late-Paleoproterozoic to the late-Mesoproterozoic, and continental collision during the Grenvillian Orogeny. This accretion occurred during several orogenies, comprising the Labradorian (ca. 1.71-1.60 Ga), the Pinwarian (ca. 1.47-1.45 Ga), the Elzevirian (ca. 1.25-1.23 Ma) and the Shawinigan (ca. 1.19-1.14 Ga). Tectono-metamorphic imprints related to the latter two are restricted to the western Grenville Province (Ketchum et al., 1994; Rivers, 1997; Rivers et al., 2012; Tucker and Gower, 1994). The Grenvillian Orogeny *sensu stricto* was caused by a continent-continent collision in the late-Mesoproterozoic to the early-Neoproterozoic (e.g. Carr et al., 2000; Hynes and Rivers, 2010; Rivers et al., 2012; Tucker and Gower, 1994). It consisted of two orogenic phases, namely the (i) Ottawa phase (ca. 1090-1020 Ma) and the (ii) Rigolet phase (ca. 1005-960 Ma), that are mainly recorded in rocks of the orogenic hinterland (Allochthonous Belt), and adjacent to the orogenic foreland (Parautochthonous Belt), respectively. The Allochthonous and Parautochthonous belts are separated by the southeast shallow-dipping and orogen-scale high-grade shear zone designated as the Allochthon Boundary Thrust (ABT) (Rivers et al., 1989, 2012).

The study area is located in the central Grenville Province (Fig. 1b) south of the Manicouagan Impact Structure (Fig. 2) in the hanging wall of the ABT. The Allochthonous and the Parautochthonous belts are of different origin and were affected by a different style of metamorphic overprint (e.g. Rivers et al., 2012). The Allochthonous Belt in this area records metamorphic ages between ca. 1070 and 1050 Ma and was subdivided into: (i) a medium to low pressure belt (aM-LP, Fig. 1b) that reached up to ca. 950 MPa and 850 °C (Dunning and Indares, 2010; Lasalle et al., 2014; Lasalle and Indares, 2014; Turlin et al., 2018); and (ii) a structurally underlying high pressure belt (aHP, Fig. 1b) that reached up to ca. 1450-1600 MPa and 860-900 °C (Indares et al., 1998; Indares and Dunning, 2001; Lasalle and Indares, 2014;

Rivers et al., 2002). The Allochthonous Belt consists of nappes, the emplacement of which has been tentatively attributed to the syn-Ottawan channel flow (e.g. Rivers, 2008). Cooling of these rocks was apparently rather slow (2 to 6 °C/Ma, Turlin et al., 2018) as documented by (i) titanite cooling ages between ca. 1006 and 987 Ma (Dunning and Indares, 2010; Indares and Dunning, 2018) and by (ii) apatite diffusion modeling leading to a closure temperature of apatite crystals of ca. 550-450 °C at ca. 960 Ma (Turlin et al., 2018).

In the footwall of the ABT in the study area, the Parautochthonous Belt records the Rigolet phase of the orogeny. It underwent a medium pressure granulite-facies peak of metamorphism between ca. 1002 and 980 Ma, at *P-T* conditions of ca. 1250-1500 MPa and ca. 815-850 °C (Hynes et al., 2000; Jannin et al., 2018a; Jordan et al., 2006; Rivers, 2009; Rivers et al., 2012; van Gool et al., 2008). These conditions were documented in the Knob Lake Group that unconformably overlie the Laurentian basement (Fig. 2, Gagnon Terrane, Hynes et al., 2000; Rivers, 1980; Rivers et al., 1989). Metapelites of this group have recorded dehydration melting of muscovite ($Ms + Qtz + Pl \rightarrow Kfs + Al_2SiO_5 + Liq.$), and subsequent dehydration melting of biotite ($Bt + Al_2SiO_5 + Qtz \rightarrow Kfs + Grt + Liq.$), both in the kyanite stability field (Jannin et al., 2018a; Jordan et al., 2006). Partial melting of these metasediments as early as ca. 1002 Ma is documented by U-Pb dating of metamorphic rims of zircon grains, which exhibit HREE-depletion and absence of negative Eu anomalies, indicating their growth in presence of peritectic garnet with no plagioclase (Jannin et al., 2018a). The retrograde *P-T* path occurred in the sillimanite stability field between 995 and 985 Ma as monazite crystallized in melt (Jordan et al., 2006) and most probably lasted until ca. 961 Ma, as indicated by synkinematic intrusion of dykes and sills of pegmatite on the southern shore of the Manicouagan Reservoir at upper and lower structural levels of the Parautochthonous and Allochthonous belts, respectively (Fig. 2, Jannin et al., 2018a). A recent reappraisal of the structural and geochronological data of the ABT showed that the down-to-the-SE Thachic shear zone (TSZ, Fig. 2) crosscuts the ABT and

deforms rocks of the Parautochthonous Belt in its footwall (Jannin et al., 2018b). Its top-to-the SE normal-sense of shear has been dated at ca. 990 Ma by U-Pb on zircon from syn-kinematic leucosome and leucogranite (Jannin et al., 2018b). These authors interpret these coeval reverse-, coaxial- and normal-sense of shear criteria at upper, middle and lower structural levels, respectively, as reflecting lateral extrusion of the partially molten Parautochthonous Belt during the Rigolet orogenic phase. Partial melting of the Parautochthonous Belt rocks started as early as ca. 1002 Ma as documented by a U-Pb zircon age on a leucosome of migmatitic paragneisses (Jannin et al., 2018a).

2.2. Isotopic signatures of the Allochthonous Belt

The study area in the Allochthonous Belt is composed of various pre-Grenvillian units, the oldest rocks being represented by the paragneisses of the Plus-Value Complex (Figs. 2 and 3), showing deposition ages around ca. 1.5 Ga that correspond to the youngest U-Pb ages on detrital zircon from a quartzite (Lasalle et al., 2013) and to the crystallization age (1497 Ma, U-Pb on zircon, Augland et al., 2015) of the intrusive Bardoux Plutonic Suite (Moukhsil et al., 2013b, 2014; Maity and Indares, 2018). Detrital zircon grains in these paragneisses yield U-Pb ages between 2.7 and 1.5 Ga, but most grains gave ages between 1.9 and 1.5 Ga (Lasalle et al., 2013). These sediments deposited in an active margin context along the southeastern boundary of Laurentia marked by the formation of continental arcs and/or back-arc basins (Augland et al., 2015; Maity and Indares, 2018) and the accretion of island arcs preserved in the Grenville Orogen, such as the Coal Creek Domain (Roback, 1996), the Escoumins supracrustal belt (Groulier et al., 2018b) or the Montauban terrane (Corrigan and van Breemen, 1997; Dunning and Indares, 2010; Sappin et al., 2009). Volcaniclastic sequences and granodiorite to granitic plutonic rocks exposed in the study area and dated at ca. 1.40-1.45 Ga are inferred to correspond to lateral equivalents of the Montauban terrane (Dunning and Indares, 2010). Detrital zircon grains of the Plus-Value Complex paragneisses point to contributions from (i) the Laurentian

margin and (ii) the Archean basement and Paleoproterozoic sequences of the Gagnon Terrane (Parautochthonous Belt) (Jordan et al., 2006; Lasalle et al., 2013; van Gool et al., 2008).

Younger pre-Grenvillian units are represented by the numerous Mesoproterozoic plutonic suites emplaced between ca. 1450 Ma and 1100 Ma, i.e. from the late-Pinwarian (ca. 1470-1450 Ma) to the post-Elzevirian (ca. 1245-1225 Ma) orogenies. They include granitic, tonalitic to dioritic orthogneisses, metamangerite, metagranite and gabbro dykes (Fig. 3, Augland et al., 2015; David et al., 2009; Gobeil et al., 2002; Moukhsil et al., 2007, 2012, 2013a, 2013b, 2014). The supra-chondritic $\epsilon\text{Hf}_{1434-1383 \text{ Ma}}$ signatures for late-Pinwarian tonalitic orthogneisses and gabbro provide evidence for their mixed crustal and mantle sources (Fig. 10, Augland et al., 2015). Among these are the Bardoux and Castoréum Plutonic Suites. The Bardoux Plutonic Suite corresponds to a metaluminous continental-arc I-type to minor peraluminous S-type metagranite emplaced into the Laurentian margin between ca. 1497 and 1488 Ma (U-Pb on zircon) with similar supra-chondritic $\epsilon\text{Hf}_{1497 \text{ Ma}}$ signatures between +2.3 and +4.7 (Fig. 10, Augland et al., 2015; Moukhsil et al., 2012, 2014). The Castoréum Plutonic Suite corresponds to metagranite associated with minor charnockite, mangerite, granitic gneisses and metatonalite emplaced at 1393 ± 8 Ma (U-Pb on zircon) in an arc-setting (Augland et al., 2015; Moukhsil et al., 2013b, 2014).

Syn- and post-Ottawan intrusions include granitic to quartz-monzodioritic orthogneisses, slightly deformed monzonitic to granitic plutonic bodies and undeformed mafic rocks (Fig. 3, David, 2006; Dunning and Indares, 2010; Moukhsil et al., 2007, 2009, 2013b, 2014). The subsequent late-Ottawan units include anorthosite, mangerite and charnockite±leuconorite±granite. The latest units are represented by the Sabot Mangerite (ca. 1017-1016 Ma) and the strongly alkalic mangerite±gabbro±syenite from the Okaopéo Plutonic Suite (1014.6 ± 2.1 Ma) with a near-chondritic $\epsilon\text{Hf}_{1015 \text{ Ma}}$ signature between -1.73 and -1.01 (Fig. 10, Augland et al., 2015; Gobeil et al., 2002; Moukhsil et al., 2007, 2009, 2013a, 2013b, 2014).

2.3. The pegmatitic granite dykes (PGD) intruding the Allochthonous Belt

Rare Earth Elements-enriched PGDs in the Allochthonous Belt of the central Grenville Province were described first by Turlin et al. (2017). These dykes intrude either paragneisses from the Plus-Value Complex (Figs. 3, 4a) or metaplutons from the Bardoux (Figs. 3, 4d) or from the Castoréum Plutonic Suites (Figs. 3, 4g). Rare-earth elements are mainly hosted in monazite in paragneiss-hosted PGDs and in allanite in metapluton-hosted PGDs (Turlin et al., 2017). All PGDs considered in this contribution show steep-dipping walls discordant to the foliation of their country rocks with no textural continuity with leucosomes and display magmatic textures with no evidence for solid-state deformation (Fig. 4, Turlin et al., 2017). However, another one from the study area studied by Turlin et al. (2018) intruded the Plus-Value Complex paragneisses at ca. 1005 Ma (Turlin et al., 2017) and presents field relationships suggesting its intrusion under close to wet-solidus temperature of its host, which is supported by apatite diffusion modeling (Turlin et al., 2018) and titanite ages (Dunning and Indares, 2010; Indares and Dunning, 2018). The PGDs were thus intruded during the progressive cooling of the Allochthonous Belt. Textural relationships between zircon and monazite in these PGDs, and Th-Si-depleted/LREE-enriched monazite cores provide evidence that zircon in these rocks was formed prior to and/or together with the LREE-bearing phases (Fig. 4c, f and i, Turlin et al., 2017).

3. Sampling and analytical methods

3.1. Sampling and preparation

One monazite-bearing PGD (13-AM-13, Fig. 4a-c) and two allanite-bearing PGDs (13-TC-5072, Fig. 4d-f, and 13-FS-1202, Fig. 4g-i) have been sampled for this study. They are located in the Universal Transverse Mercator (UTM) zone 19 at the coordinates E512052-N5614036 (13-AM-13 monazite-bearing PGD), E510668-N5603384 (13-TC-5072 allanite-

bearing PGD) and E510162-N5601234 (13-FS-1202 allanite-bearing PGD) (Moukhsil et al., 2014; Turlin et al., 2017). These dykes display a variety of facies defined in particular by the heterogeneous distribution of accessory minerals including zircon. We chose to sample representative facies of these three PGDs with an intermediate grain size and content in accessory minerals as presented by Turlin et al. (2017).

Separation of heavy minerals was performed at GeoRessources (Nancy, France). Hand specimens of PGDs were crushed using a jaw and a roll crusher. The heavy fractions were then separated by classical density techniques (bromofom: density = 2.87 g/cm³) and zircon grains of various shapes and sizes (up to 2,500 µm) were handpicked under binocular microscope. The most representative crystals were mounted on an epoxy mount and characterized by means of back scattered electron (BSE) imaging performed at Goethe University Frankfurt (Germany). Inherited cores were not observed and porous domains were avoided during analyses.

3.2. U-Pb dating and Lu-Hf isotope analyses of zircon

In-situ U-Pb and Lu-Hf isotopes analyses were carried out on nineteen zircon grains from the monazite-bearing PGD. From the allanite-bearing PGDs, fourteen zircon grains were analyzed from sample 13-TC-5072, and twenty-five from sample 13-FS-1202. Analyses were carried out by laser ablation-inductively coupled plasma-sector field-mass spectrometry (LA-ICP-SF-MS) at Goethe University Frankfurt (Germany), using methods and instruments as described by Gerdes and Zeh (2006, 2009), with modifications explained in Zeh and Gerdes (2012). Laser spots for Lu-Hf isotope analyses (round spots with a size of 64-100 µm) were placed on-top of U-Pb laser spots (round spots with a size of 20-42 µm). Detailed analytical methods of U-Pb dating and Lu-Hf isotopes analyses and results are provided in Supplementary material and in Tables S1 and S2, respectively.

3.3. Trace element analyses of zircon

Among zircon analyzed for their U-Pb-Hf isotopic signature, eleven grains from the monazite-bearing PGD, thirteen from the 13-TC-5072 sample and fifteen from the 13-FS-1202 allanite-bearing PGDs were selected for trace element analyses.

In-situ trace element analyses were carried out by using LA-SF-ICP-MS at Goethe University Frankfurt (Germany). Laser spots (round spots with a size of 42 μm) were placed on representative domains of the investigated grains, when possible as close as possible to U-Pb and Lu-Hf laser spots. For this study, the following isotopes have been analyzed: ^{44}Ca , ^{49}Ti , ^{57}Fe , ^{89}Y , ^{139}La , ^{140}Ce , ^{141}Pr , ^{146}Nd , ^{147}Sm , ^{151}Eu , ^{158}Gd , ^{159}Tb , ^{161}Dy , ^{165}Ho , ^{167}Er , ^{169}Tm , ^{172}Yb , ^{175}Lu , ^{232}Th and ^{238}U . Detailed analytical methods of trace element analyses and results are provided in Supplementary material and in Table S3, respectively.

3.4. O isotope analyses of zircon

Among zircon analyzed for their U-Pb-Hf isotopic signature, fourteen grains from the monazite-bearing PGD, all zircon grains from the 13-TC-5072 sample and seventeen grains from the 13-FS-1202 allanite-bearing PGD were selected for O isotopes analyses.

In-situ ion probe oxygen isotopes analyses were performed with the Cameca IMS 1280 HR2 ion microprobe at the Centre de Recherches Pétrographiques et Géochimiques (CRPG, Nancy, France), following Martin et al. (2008). The Cs^+ primary ion beam of 5 to 7 nA was focused on a 20 μm diameter area and the electron gun used for the charge compensation. The negative secondary ions were measured with a mass resolution of 4400 ($M/\Delta M$) with an energy slit of 35 eV. Before each measurement, the sample was pre-sputtered for 60 s with a beam rastering on 10 μm to clean up the sample surface, then the secondary beam was automatically centered in the field aperture and contrast aperture. The measurements were made on Faraday cups in multicollection mode with counting time of 120 s. The instrumental mass fractionation was determined on the reference zircon 91500. The results are shown in Table S4.

4. Results

4.1. Zircon textures

Zircon grains from the 13-AM-13 monazite-bearing PGD sample can be subdivided into two groups. Grains comprising the dominant zircon population are characterized by oscillatory zoning, which was locally affected by dissolution, prior to overgrowth. These grains have length between 400 and 2200 μm and elongated sub-moderate aspect ratios of about 1:2 (Figs. 5a and 6a). They display prismatic shapes with dominant (100) and (110) crystal faces and subrounded terminations. A minor zircon population is characterized by a complex, non-systematic zoning (Figs. 5a and 6a). It mostly comprises small grains with length ranging from 350 to 850 μm , and aspect ratios at 1:2, rarely down to 1:1.

Zircon grains in the 13-TC-5072 allanite-bearing PGD sample can also be divided into two groups. The dominant population is characterized by an oscillatory zoning locally interrupted by dissolution textures (Figs. 5b and 6b). The grains show elongations between 250 and 700 μm , moderate aspect ratios between 1:1 and 1:3, and prismatic shapes with predominantly (100) and (110) crystal faces and subrounded terminations. A minor population reveals a typical sector (hourglass) zoning (Figs. 5b and 6b). Elongation of these grains ranges between 350 and 750 μm , and aspect ratios between 1:2 and 1:3.

Zircon grains in the 13-FS-1202 allanite-bearing PGD sample can be divided into four groups. The 'oscillatory zoning' population is characterized by a fine zoning and comprises rounded to elongated sub-euhedral grains with length comprised between ca. 600 and 700 μm , and moderate aspect ratios ranging from 1:1 to 1:3 (Figs. 5c and 6c). The 'complex zoning' population is composed of rounded to elongated sub-euhedral grains, with lengths ranging from 300 to 850 μm , and aspect ratios between 1:1 and 1:3 (Figs. 5c and 6c). The 'hourglass zoning' population shows a typical sector zoning in BSE images, and is composed of elongated sub-

ehedral grains with length between 550 and 2500 μm , and moderate aspect ratios ranging from 1:2 to 1:3 (Figs. 5c and 6c). The ‘banded zoning’ population comprises elongated sub-ehedral grains having lengths between ca. 900 and 2100 μm , and aspect ratios ranging from 1:2 to 1:3 (Figs. 5c and 6c).

4.2. Trace elements

In this study, textural observations are combined with chemical characteristics to distinguish pristine from non-pristine, altered zircon domains, using similar criteria as described in detail in Zeh et al. (2014). Altered zircon grains/domains are commonly characterized by high contents in large ionic radii/low ionic charge trace element that do not fit in the zircon lattice, comprising Ca, Fe and LREE (mainly La). These can occur as nanoscale pores fillings or micrometric inclusions in fractured, porous or metamict domains (e.g. Geisler et al., 2001, 2007; Hanchar et al., 2001; Hoskin and Schaltegger, 2003; Martin et al., 2008; Seydoux-Guillaume et al., 2015; Zeh et al., 2014). Such domains often show U-Pb discordance and elevated common Pb contents (e.g. Geisler et al., 2007; Martin et al., 2006, 2008; Pidgeon, 1992; Rayner et al., 2005). In this study pristine domains are defined on the basis of ΣLREE and Ca+Fe contents below 30 ppm and 100 ppm, respectively (Fig. 7a, Table 1). Zircon domains with higher contents are defined as non-pristine and designated as ‘*LREE-Ca-Fe-rich*’.

4.2.1. Monazite-bearing PGD (sample 13-AM-13)

Zircon grains in the monazite-bearing PGD mostly have a pristine character ($n = 26$) with ΣLREE below 23 ppm, Ca below 94 ppm and Fe below 11 ppm contents (Fig. 7a, Table 1). The Th/U ratios and ΣHREE contents of the analyzed domains range from 0.16 to 0.60 and from 197 to 825 ppm (Fig. 7b, Table 1), respectively, and the chondrite-normalized REE patterns are all very similar (Fig. 7f). They reveal a (i) strong fractionation of the HREE over the LREE ($\text{Yb}_\text{N}/\text{Sm}_\text{N}$ ranging from 34 to 64), (ii) positive Ce (Ce/Ce^* from 3.39 to 37.49) and

(iii) negative Eu (Eu/Eu^* from 0.04 to 0.08) anomalies, and (iv) a progressive increase in the HREE ($\text{Yb}_\text{N}/\text{Gd}_\text{N}$ from 9.4 to 15) (Fig. 7f, Table 1). Steep LREE slopes in the chondrite-normalized patterns are marked by high $\text{Sm}_\text{N}/\text{La}_\text{N}$ ratios generally ranging from 163 to 2268 (Figs. 7c, f, Table 1; exception is reported for the grain 1-10, zone 2 with a ratio of 59). The Th, U, Y and Yb contents of these domains range from 40 to 311 ppm, from 246 to 756 ppm, from 285 to 1324 ppm and from 81 to 302 ppm (Table 1), respectively.

The non-pristine zircon domains (LREE-Ca-Fe-rich) in the monazite-bearing PGD ($n = 13$) show higher contents of LREE, Ca and Fe up to 115 ppm, 7816 ppm and 96 ppm (Fig. 7a, Table 1), respectively, a slightly reduced negative Eu anomaly (Eu/Eu^* up to 0.17), and higher Th (up to 820 ppm) and U contents (up to 1374 ppm), resulting in higher Th/U ratios (up to 1.43) (Figs. 7b, d, f, Table 1). These domains also show flatter chondrite-normalized LREE patterns with $\text{Sm}_\text{N}/\text{La}_\text{N}$ ratio down to 4.7 and less pronounced Ce anomalies (Ce/Ce^* down to 0.98, Figs. 7c, f, Table 1). The ΣHREE (from 238 to 1194 ppm), $\text{Yb}_\text{N}/\text{Sm}_\text{N}$ ratios (from 4.6 to 54, Fig. 7f), and the Y (from 325 to 1767 ppm) and Yb (from 94 to 414 ppm) contents are similar to those of the pristine domains (Table 1).

Pristinity or non-pristinity is not correlated to specific zircon groups or textural domains described in the previous section (Figs. 5a and 6a). In the U/Yb vs Y (ppm) diagrams of Grimes et al. (2007), data from pristine and LREE-Ca-Fe-rich domains both plot in the field for continental rocks (Fig. 7e).

4.2.2. Allanite-bearing PGD (samples 13-TC-5072 and 13-FS-1202)

Zircon grains from sample 13-TC-5072 mostly show a pristine character ($n = 19$) with ΣLREE below 22 ppm, Ca below 83 ppm, and Fe below 11 ppm (Fig. 7a, Table 1). The Th/U ratios and ΣHREE contents of these pristine domains range from 0.07 to 0.40 and from 146 to 906 ppm (Fig. 7b, Table 1), respectively. These domains show similar chondrite-normalized

REE patterns with a (i) strong fractionation of the HREE over the LREE (Yb_N/Sm_N ranging from 29 to 206), (ii) positive Ce (Ce/Ce^* from 2.20 to 214.88) and (iii) negative Eu (Eu/Eu^* from 0.06 to 0.09) anomalies, (iv) Yb_N/Gd_N from 8 to 38, and (v) variable Sm_N/La_N ratios ranging from 4 to 1728 (Figs. 7c, g, Table 1). The Th, U, Y and Yb contents of these domains range from 15 to 162 ppm, from 148 to 502 ppm, from 165 to 1347 ppm and from 71 to 363 ppm (Table 1), respectively.

The non-pristine domains (LREE-Ca-Fe-rich) of zircon grains in sample 13-TC-5072 ($n = 13$) show higher contents of incompatible LREE, Ca and Fe of 1274 ppm, 474 ppm and 1215 ppm (Table 1), respectively, and of Th and U up to 236 ppm and 741 ppm, respectively, and somewhat lower Eu negative anomalies (Eu/Eu^* up to 0.16, Figs. 7b and g, Table 1). The chondrite-normalized REE patterns are flatter than those of the pristine domains as indicated by Yb_N/Sm_N down to 9 and Sm_N/La_N down to 0.1 (Figs. 7c, g, Table 1), and the less pronounced Ce anomalies with Ce/Ce^* down to 0.76 (Fig. 7g, Table 1). The Th/U ratio (from 0.24 to 0.36), Σ HREE (from 185 to 892 ppm), Y (from 252 to 1385 ppm), and Yb (from 80 to 349 ppm) contents are similar to pristine domains (Figs. 7b, e, g, Table 1).

Both zircon groups, distinguished by their textures, contain pristine and non-pristine zircon domains (Figs. 5b and 6b). In the U/Yb vs Y diagram of Grimes et al. (2007), pristine and non-pristine domains plot in the field for continental rocks (Fig. 7e).

Pristine and non-pristine zircon grains in sample 13-FS-1202 show very similar compositions like those of sample 13-TC-5072 (Figs. 7a-c, e, h, Table 1). Also their chemical characteristics (pristine vs. non-pristine) cannot be attributed to specific zircon groups or textural zones (Figs. 5c and 6c).

4.3. Ti-in-zircon temperatures

The pristine zircon domains of the monazite-bearing PGD have Ti contents ranging from 3.8 to 7.6 ppm, and those in the two allanite-bearing PGDs between 1.1 to 4.3 ppm (Table 1), corresponding to zircon crystallization temperatures between 662 and 721 °C for the monazite-bearing PGD, and between 667 and 716 °C (sample 13-TC-5072) and between 640 and 685 °C (sample 13-FS-1202) for the allanite-bearing PGDs (Fig. 7d, Table 1). One pristine zircon domain from sample 13-TC-5072 yields a significantly lower temperature of 608°C (Fig. 7d, Table 1). The zircon crystallization temperatures were calculated with the Ti-in-zircon thermometer calibrated by Ferry and Watson (2007), using the following activities for SiO₂ (quartz) and TiO₂ (rutile): $a(\text{SiO}_2) = a(\text{TiO}_2) = 1$ for the monazite-bearing rocks, and $a(\text{SiO}_2) = 1$ and $a(\text{TiO}_2) = 0.6$ for the allanite-bearing PGDs. The different activities for TiO₂ reflect the presence or lack of Ti-oxides in the monazite- and allanite-bearing PGDs (Hayden and Watson, 2007), respectively, as described by Turlin et al. (2017).

4.4. Oxygen isotopes

Ninety-one O isotopes analyses were carried out on fifteen zircon grains from the monazite-bearing sample 13-AM-13 (Fig. 8, Table 1). Eighty-five analyses yield supra-mantle (>5.3 ‰ as defined by Valley et al., 2005) $\delta^{18}\text{O}_{\text{V-SMOW}}$ values ranging between +5.91 and +9.52 ‰ (individual error below ± 0.18 ‰, 2 S.D.; mean: +7.65 ‰; Fig. 8a, Table 1). Zircon grains with complex zoning (Figs. 5a and 6a) show very similar supra-mantle $\delta^{18}\text{O}_{\text{V-SMOW}}$, whereas zircon grains with oscillatory zoning can record variations in supra-mantle $\delta^{18}\text{O}_{\text{V-SMOW}}$ up to ca. 3 ‰ (e.g. grains 1-6, Figs. 5a and 6a, Table 1). Six analyses yield mantle to sub-mantle $\delta^{18}\text{O}_{\text{V-SMOW}}$ values between +0.69 and +5.33 ‰ (individual error below ± 0.28 ‰, 2 S.D.; mean: +3.58 ‰; Fig. 8a, Table 1). Such low values were obtained exclusively by rim analyses of grain 1-3, and by core and rim analyses of grain 1-17 (Figs. 5a and 6a, Table 1).

Fifty-one O isotopes analyses were carried out on fourteen zircon grains from the allanite-bearing PGD sample 13-TC-5072 (Fig. 8, Table 1). Forty-nine analyses yield supra-mantle $\delta^{18}\text{O}_{\text{V-SMOW}}$ values, ranging mainly from +5.92 to +7.80 ‰ (n = 46; individual error below ± 0.19 ‰, 2 S.D.; mean: +6.79 ‰; Fig. 8a, Table 1). Three analyses from an oscillatory zoned zircon (grain 3-12, Figs. 5b and 6b) yield higher $\delta^{18}\text{O}_{\text{V-SMOW}}$ values, ranging from +12.57 to +15.04 ‰ (mean +13.55 ‰, Table 1). Two mantle-like $\delta^{18}\text{O}_{\text{V-SMOW}}$ values of +5.04 and +5.31 ‰ (individual error below ± 0.16 ‰, 2 S.D.; Fig. 8a, Table 1) are recorded in grains 3-6 and 3-14 showing an hourglass zoning, even though most grains from the population with “hourglass zoning” are characterized by higher values. In general, the $\delta^{18}\text{O}_{\text{V-SMOW}}$ values are very homogeneous within single zircon grains of sample 13-TC-5072 (Table 1).

From the allanite-bearing PGD sample 13-FS-1202 seventy-four O isotopes analyses were carried out on seventeen zircon grains. Data from this sample are highly variable (Fig. 8, Table 1). Forty-four analyses yield supra-mantle $\delta^{18}\text{O}_{\text{V-SMOW}}$ values ranging between +5.87 and +10.26 ‰ (individual error below ± 0.37 ‰, 2 S.D.; mean +7.58 ‰; Fig. 8a, Table 1). Two analyses yield mantle-like $\delta^{18}\text{O}_{\text{V-SMOW}}$ values of +5.06 and +5.08 ‰ (individual error below ± 0.13 ‰), and twenty-eight analyses yield sub-mantle $\delta^{18}\text{O}_{\text{V-SMOW}}$ values between -1.65 and +4.90 ‰ (individual error below ± 0.42 ‰; mean: +1.77 ‰; Fig. 8a, Table 1). The $\delta^{18}\text{O}_{\text{V-SMOW}}$ values can be highly variable within single zircon grains, and also rather homogeneous in others. Enormous variations are shown by grain 2-21 ($\delta^{18}\text{O}_{\text{V-SMOW}}$ from -1.63 to +9.20 ‰; error = ± 0.24 ‰, 2 S.D.), and homogenous supra-mantle signatures between +8.21 and +10.26 ‰ by the grains 2-7, 2-8, 2-9 and 2-15, whereas grain 2-24 only shows strongly sub-mantle $\delta^{18}\text{O}_{\text{V-SMOW}}$ values ranging from -1.65 to +1.02 (Figs. 5c and 6c, Table 1). The variations in the $\delta^{18}\text{O}_{\text{V-SMOW}}$ signatures are not correlated to zircon textures. Furthermore, it is pertinent to note that

variations in $\delta^{18}\text{O}_{\text{V-SMOW}}$ values are not correlated to Ca and Fe contents (Fig. 8b), suggesting that most of these variations are unrelated to post-intrusive zircon alteration.

4.5. U-Pb dating

From the monazite-bearing PGD sixty-seven U-Pb isotopes analyses on nineteen zircon grains were carried out on both pristine and non-pristine domains, and from the allanite-bearing PGDs, thirty-six on fourteen grains of sample 13-TC-5072, and seventy-four on twenty-five grains of sample 13-FS-1202 (Figs. 5 and 6, Table 1). Most analyses are concordant, and yield, within error identical concordia ages for all three samples: 1004.2 ± 2.1 Ma ($n = 48$, Fig. 9a), 1001.9 ± 3.9 Ma ($n = 14$, Fig. 9b), and 1004.2 ± 2.3 Ma ($n = 42$, Fig. 9c), respectively. The degree of concordance is not correlated to the LREE, Ca and Fe content (Figs. 9d and e).

4.6. Lu-Hf isotopes

Fifty-nine Lu-Hf isotope analyses were carried out on zircon grains from the monazite-bearing PGD, and from the allanite-bearing PGDs thirty-six on zircon from sample 13-TC-5072, and seventy-three from sample 13-FS-1202 (Figs. 5 and 6).

Pristine and non-pristine zircon domains from the monazite-bearing PGD yield within error identical initial $^{176}\text{Hf}/^{177}\text{Hf}_{(1003\text{ Ma})}$ of 0.281981 ± 0.000036 (2 S.D, $n = 59$), corresponding to $\epsilon\text{Hf}_{(1003\text{ Ma})}$ of -6.1 ± 1.5 , and hafnium model ages (T_{DM2}) of 2.12 ± 0.07 Ga (Fig. 10, Table 1). These ratios and values are slightly higher than those obtained from the allanite-bearing PGD samples 13-TC-5072 ($^{176}\text{Hf}/^{177}\text{Hf}_{(1003\text{ Ma})} = 0.281865 \pm 0.000054$ (2 S.D, $n = 36$); $\epsilon\text{Hf}_{(1003\text{ Ma})} = -10.0 \pm 1.8$; $T_{DM2} = 2.34 \pm 0.10$ Ga), and 13-FS-1202 ($^{176}\text{Hf}/^{177}\text{Hf}_{(1003\text{ Ma})} = 0.281931 \pm 0.000042$ (2 S.D, $n = 73$); $\epsilon\text{Hf}_{(1003\text{ Ma})} = -7.8 \pm 1.4$; $T_{DM2} = 2.21 \pm 0.08$ Ga) (Fig. 10, Table 1).

5. Discussion

5.1. Timing and conditions of zircon crystallization in monazite- and allanite-bearing PGDs

Zircon in the monazite- and allanite-bearing PGDs are mostly pristine, lack evidence for inherited cores and only locally display textures of dissolution-reprecipitation (Figs. 5, 6 and 7a, see sections 4.1. and 4.2. for details). Textures and chemical compositions argue in favor of an igneous origin of most zircon grains during crystallization of the PGDs (e.g. Corfu et al., 2003; Crowley et al., 2008; Rubatto, 2017). This interpretation is supported by (i) their generally low LREE, Ca and Fe contents, by (ii) their chondrite-normalized REE patterns characterized by an increase from LREE to HREE, and pronounced Ce anomalies, and (iii) high Th/U ratios (Figs. 7f-h, e.g. Bea, 1996; Grimes et al., 2007). Non-pristine zircon domains are associated with a flattening of the LREE in the chondrite-normalized patterns (Figs. 7c, f-h, Table 1) that is correlated with an increase in Th and U contents, and Th/U ratios in the monazite-bearing PGD, and with an increase in Ca, Fe and Σ LREE contents in the allanite-bearing PGDs (Figs. 7a-b, Table 1). Systematic high resolution SEM images of non-pristine domains did not allow to identify nanoscale pores fillings and/or inclusions of such incompatible elements in the zircon lattice that may have been sampled in the laser spots and/or beneath the surface of the analyzed zircon. The PGDs host LREE either in monazite $[(\text{Ce}, \text{La}, \text{Nd}, \text{Th})\text{PO}_4]$ or allanite $[(\text{Ce}, \text{Ca})_2(\text{Al}, \text{Fe}^{3+})_3(\text{SiO}_4)_3(\text{OH})]$ both formed together with or after zircon (Turlin et al., 2017). Crystallization of magmatic monazite immediately after zircon crystallization is suggested by U-Pb ages of zircon (1004 ± 2 Ma, Fig. 9a, this study) and monazite (1005 ± 4 Ma – 997 ± 5 Ma, Turlin et al., 2017) that overlap within error. Furthermore, non-pristine zircon domains of monazite-bearing PGD show Th and U contents and Th/U ratios that are higher than (i) pristine domains, therefore mimicking the composition of monazite grains (Turlin et al., 2017), and higher than (ii) non-pristine ones from allanite-bearing PGD (Fig. 7a, Table 1). These features suggest that the alteration of most zircon domains was

associated with infiltration of LREE, Ca, Fe, U and Th, and occurred immediately after zircon crystallization coeval with monazite crystallization. The same is likely for zircon in the allanite-bearing PGDs even though allanite is not dated. This implies that alteration must have occurred by a coupled dissolution-precipitation, causing the formation of nanopores subsequently filled with zircon-incompatible trace element, and not by diffusion or recrystallization processes after metamictization of the zircon grains, as there has been no time for a serious damage of the zircon lattice. The driving force for this dissolution-precipitation was probably the incorporation of relatively high amounts of large ionic elements like Th, U and REE, during cooling of the zircon grains initially formed at high temperatures and that caused lattice strain (see Geisler et al., 2007). This interpretation is in agreement with that of Turlin et al. (2018), who concluded to the intrusion of monazite-bearing PGDs into their metasedimentary hosts under close to wet-solidus conditions of ca. 650-700 °C (see section 2.3. for details). This is supported by the estimated crystallization temperatures of zircon grains of 662-721 °C for the monazite-bearing PGD, and 667-716 °C (sample 13-TC-5072) and 640-685 °C (sample 13-FS-1202) for the allanite-bearing PGDs (Fig. 7d, Table 1). In summary, identical crystallization ages of 1004.2 ± 2.1 Ma (sample 13-AM-13), 1001.9 ± 3.9 Ma (sample 13-TC-5072), and 1004.2 ± 2.3 Ma (sample 13-FS-1202), and similarities in the structural setting, and in the textural, geochemical and petrological characteristics suggest that the Mnz- and Aln-bearing PGDs were emplaced and crystallized coevally (see Turlin et al., 2017). The new zircon U-Pb ages (Figs. 9a-c) confirm the emplacement age of ca. 1005-1000 Ma, obtained by Turlin et al. (2017) on monazite of sample 13-AM-13, providing additional evidence for the coeval intrusion of steeply dipping monazite- and allanite-bearing PGDs from the Lac Okaopéo region (central Grenville Province).

Zircon grains, designated to be pristine, in both the monazite- and allanite-bearing PGDs mostly show supra-mantle $\delta^{18}\text{O}_{\text{V-SMOW}}$ signatures between +5.91 and +9.52 ‰ (mean of +7.65

‰) and between +5.92 and +7.80 ‰ (mean of +6.79 ‰) (Fig. 8a, Table 1), respectively. Such values are commonly attributed to a melt issued from partial melting of metasedimentary rocks consistent with the peraluminous character of the PGDs (Turlin et al., 2017; Valley, 2003; Valley et al., 2005). However, some grains or domains show sub-mantle values down to -1.9‰, pointing to a distinct fluid source, perhaps triggered by interaction of metamict zircon domains (or along fractures) with cold surface water (e.g. Valley, 2003; Valley et al., 2005) during near-surface weathering (see Pidgeon et al., 2013).

The relatively wide range in supra-mantle $\delta^{18}\text{O}_{\text{V-SMOW}}$ obtained from zircon grains in all investigated samples (Figs. 5, 8, Table 1) might reflect either (i) a heterogeneous magma with respect to the oxygen isotopes by the time of zircon crystallization, due to incomplete homogenization of the magma composition or to a heterogeneous source, (ii) a result of zircon alteration through a coupled dissolution-precipitation immediately after zircon crystallization, or (iii) a mixed effect including weathering (for low $\delta^{18}\text{O}_{\text{V-SMOW}}$). The first hypothesis seems unlikely, considering the fact that the initial Hf isotopic composition ($^{176}\text{Hf}/^{177}\text{Hf}_{(1003\text{ Ma})}$ ratio) of all zircon grains/domains in the investigated PDGs is mostly identical within error (Table 1). This suggests that (i) even if the PDG melt(s) were derived from a heterogeneous source, their composition was homogeneous at the time of zircon crystallization, and that (ii) the melt(s) did not contain any inherited zircon (in agreement with the textural observations) that would have preserved its original $^{176}\text{Hf}/^{177}\text{Hf}$ and $\delta^{18}\text{O}_{\text{V-SMOW}}$ (Valley et al., 2005; Zeh et al., 2014). The absence of inherited zircon grains is counterintuitive with the peraluminous signature of the melts that are formed by low temperatures of partial melting (ca. 650-750 °C) of older crust, allowing the preservation of inherited zircon domains, as is, for example, well demonstrated by zircon in the S-type Cape Granite Suite in South Africa (Farina et al., 2014; Villaros et al., 2012). The absence of such inherited zircon in the investigated PDGs samples could be explained either by (i) melting of sedimentary rocks having very low Zr contents, resulting in

the complete dissolution of older grains during melting (see Watson & Harrison, 1983), or by (ii) the retention of zircon in their protolith(s) during melt extraction (see Watt et al., 1996), causing a significantly different $^{176}\text{Hf}/^{177}\text{Hf}$ zircon signature compared to the source rock as zircon is a major Hf-bearing mineral (e.g. Gerdes and Zeh, 2009; Tang et al., 2014). Data presented in this study do not allow to argue in favor of one or another hypothesis.

Taking all these options into account, the variations in supra-mantle $\delta^{18}\text{O}_{\text{V-SMOW}}$ values are most likely explained by zircon alteration due to coupled dissolution-reprecipitation immediately after zircon crystallization, during cooling of the dykes. This interpretation is in agreement with the observation that many of the zircon domains with supra-mantle $\delta^{18}\text{O}_{\text{V-SMOW}}$ also show a diffuse zoning and micropores (Fig. 5). The variations in sub-mantle $\delta^{18}\text{O}_{\text{V-SMOW}}$ might result either from (i) different amounts of heavy oxygen, bounded in nanopores formed during the dissolution-reprecipitation, and/or (ii) fractionation between aqueous fluids and solid phases during cooling (see Valley, 2003).

5.2. Source of the PGD magmas

Late-Ottawan magmatism is marked, in the study area, by the intrusion of the ca. 1020-1015 Ma Sabot Mangerite and Okaopéo Plutonic Suite into the Allochthonous Belt (Augland et al., 2015; Gobeil et al., 2002; Moukhsil et al., 2014). The high-alkalic components of these magmas led Augland et al. (2015) to propose that they were emplaced during the late-Ottawan crustal thinning/extension inferred to represent orogenic collapse preceding the Rigolet tectonic-metamorphic phase (Moukhsil and Solgadi, 2018a, 2018b; Rivers, 2012). Augland et al. (2015) reported a slightly sub-chondritic $\varepsilon\text{Hf}_{(1015\text{ Ma})}$ signature ranging from -1.73 and -1.01 for a mangerite sample of the ca. 1015 Ma Okaopéo Plutonic Suite, and supra-chondritic $\varepsilon\text{Hf}_{(1383-1497\text{ Ma})}$ signatures of pre-Grenvillian allochthonous plutonic units that include tonalitic orthogneisses, gabbro-norite dykes and granitic samples from the Lac Okaopéo region (Fig. 10).

Altogether, they define a crustal evolution domain (with $^{176}\text{Lu}/^{177}\text{Hf} = 0.015$) with a lower limit marked by the Bardoux's signature (Fig. 10, Augland et al., 2015). They correspond to Hf model ages ranging from 1.46 Ga (tonalitic orthogneisses) to 2.10 Ga (Bardoux Plutonic Suite) (Fig. 10, Augland et al., 2015). Zircon grains from the monazite- and allanite-bearing PGDs yield $\varepsilon\text{Hf}_{(1003\text{ Ma})}$ ranging from -4.7 to -7.6, and from -6.4 to -11.8, respectively, corresponding to Hf model ages of 2.05-2.19 Ga, and 2.13-2.44, respectively (Fig. 10). These model ages are significantly older than those obtained from all Grenvillian and pre-Grenvillian plutonic units of the Allochthonous Belt from the Lac Okaopéo region reported by Augland et al. (2015). This indicates that the PGDs have been derived from an older crustal component extracted from a depleted mantle source during the late-Archean to early-Paleoproterozoic.

Protoliths older than allochthonous plutonic units and compatible with the Paleoproterozoic $T_{DM2(1003\text{ Ma})}$ Hf model ages yielded by zircon from the Allochthonous Belt-hosting PGDs of the central Grenville Province are represented in this area by (i) the Plus-Value Complex paragneisses in the Allochthonous Belt (Lasalle et al., 2013; Moukhsil et al., 2014), and by (ii) rocks of the Gagnon Terrane in the underlying Parautochthonous Belt that include the Knob Lake Group metapelites and its tonalitic Archean basement (Jordan et al., 2006). The U-Pb ages of zircon cores from the Plus-Value Complex paragneisses range from ca. 1.5 to 2.7 Ga, and mainly between ca. 1.9 and 1.5 Ga (Lasalle et al., 2013; Moukhsil et al., 2014). This large scattering reflects a potential variable range of sources, which is line with the diversity of terranes accreted along the southeastern Laurentia active margin from the late-Paleoproterozoic and throughout the Mesoproterozoic (Corrigan and van Breemen, 1997; Dunning and Indares, 2010; Groulier et al., 2018b; Rivers et al., 2012; Roback, 1996; Sappin et al., 2009). Zircon grains from the Plus-Value Complex paragneisses also present two pre-Grenvillian overgrowths dated at ca. 1.4 Ga, 1.2 Ga, and one syn-Ottawan overgrowth dated at ca. 1.08-1.04 Ga (Lasalle et al., 2013). No Hf isotope data on these zircon grains are available in the

literature but one would expect that their partial melting up to complete dissolution of inherited zircons (compatible with the lack of inherited cores in zircon from the PGDs) should generate magmas with (i) more heterogeneous and (ii) higher $\epsilon\text{Hf}_{(1003\text{ Ma})}$ signatures, and (iii) younger $T_{DM2\ (1003\text{ Ma})}$ Hf model ages than that obtained in this study on zircon grains from the PGDs. Alternatively, a low-degree of partial melting under low-temperature would allow the preservation of zircon grains in the protolith and the genesis of magmas without inherited zircon cores/domains. However, during such process and due to the low Lu/Hf and $^{176}\text{Hf}/^{177}\text{Hf}$ ratios of zircon grains, zircons that are unentrained in the melts during anatexis lead to a significant retention of ^{177}Hf in the source (e.g. Gerdes and Zeh, 2009; Tang et al., 2014). Therefore, melts produced have higher $^{176}\text{Hf}/^{177}\text{Hf}$ ratios, and $\epsilon\text{Hf}_{(t)}$, than the source. Accordingly, the $\epsilon\text{Hf}_{(1003\text{ Ma})}$ yielded by zircon grains from the PGDs correspond to a maximum proxy of the $\epsilon\text{Hf}_{(1003\text{ Ma})}$, and conversely minimum Hf model ages, of the source. In addition, (i) the monazite-bearing PGD shows intrusive contact into the Plus-Value Complex paragneisses with no textural continuity with concordant leucosomes (Fig. 4a), and (ii) partial melting of these paragneisses was initiated as early as ca. 1080 Ma and reached a climax between ca. 1070 and 1050 Ma during the Ottawa peak of metamorphism (Lasalle et al., 2014; Lasalle and Indares, 2014; Turlin et al., 2018). By the time of PGDs' intrusion at ca. 1005-1000 Ma (Fig. 9a-c, U-Pb on zircon, this study; and on monazite, Turlin et al., 2017), the allochthonous crustal segment hosting the PGDs underwent slow cooling down to close to solidus conditions (Turlin et al., 2018). Even though from data presented in this study we cannot dismiss an early-Rigolet contribution of the Plus-Value Complex from structurally lower segments in the genesis of the PGDs, based on the evidence discussed above we exclude their derivation by partial melting of this allochthonous unit at the structural level of emplacement.

The Rigolet orogenic phase started at ca. 1005-1000 Ma in the Parautochthonous Belt (e.g. Krogh, 1994; Rivers, 2008, 2009; Rivers et al., 1989, 2012), i.e. at the time of emplacement

of the PGDs in the Allochthonous Belt (this study; Turlin et al., 2017). The Rigolet phase was recorded in the central Grenville Province in metapelites from the Knob Lake Group (Gagnon Terrane, pMP, Figs. 1b and 2) as a peak of metamorphism up to granulite-facies conditions at ca. 1250-1500 MPa and ca. 815-850 °C (Hynes et al., 2000; Jannin et al., 2018a; Jordan et al., 2006; Rivers, 2009; Rivers et al., 2012; van Gool et al., 2008). The Rigolet metamorphism was associated with deformation phases in the presence of melt as early as ca. 1002 Ma and with a cooling down to ca. 700-600 °C around 960 Ma (Jannin et al., 2018a; Jordan et al., 2006). Accordingly, favorable conditions for partial melting in the outcropping areas of the Gagnon Terrane (i.e. north of the study area, Fig. 2) and for the generation of the PGD magmas hosted in the Allochthonous Belt were reached as early as ca. 1002 Ma. Coupled with the Hf isotope analyses on zircon grains, these features point to the derivation of the PGDs by the partial melting of rocks from the Parautochthonous Belt.

Magmatic zircon grains from the Grenville Province generally show higher and more variable $\delta^{18}\text{O}_{\text{V-SMOW}}$ signatures (8.2 ± 1.7 ‰) than igneous zircon from the Superior Province (5.7 ± 0.6 ‰) providing evidence for the dramatic increase in the recycling of the Grenvillian crust through the subduction of supracrustal sequences (e.g. King et al., 1998; Valley, 2003; Valley et al., 2005; Van Kranendonk and Kirkland, 2013). The O isotope analyses carried out in zircon from the monazite- and the 13-TC-5072 allanite-bearing PGDs are dominated by supra-mantle $\delta^{18}\text{O}_{\text{V-SMOW}}$ signatures (i.e. above the range 5.3 ± 0.3 ‰, as defined by Valley et al., 2005) between +5.91 and +9.52 ‰ (mean of +7.65 ‰) and between +5.92 and +7.80 ‰ (mean of +6.79 ‰) (Fig. 8a, Table 1), respectively. Such values are commonly attributed to a supracrustal source of the melt consistent with the peraluminous character of the PGDs (Turlin et al., 2017; Valley, 2003; Valley et al., 2005). In addition, both pristine and non-pristine zircon domains show Y, U and Yb contents typical of zircon from continental rocks as defined by Grimes et al. (2007). These features, together with the trace elements, the $\varepsilon\text{Hf}_{(1003 \text{ Ma})}$ values

and the T_{DM2} (1003 Ma) Hf model ages of zircon grains, and the peraluminous character of the PGDs (Turlin et al., 2017) strengthen the model of pluton unrelated genesis of the Sveconorwegian (Scandinavian extension of the Grenville Province) Evje-Iveland pegmatites from southern Norway (Müller et al., 2015). Indeed, they indicate that PGDs from the central Grenville Province were formed by partial melting of Paleoproterozoic-Archean sedimentary material from the Laurentian margin, represented in this area of the Parautochthonous Belt by the Knob Lake Group metapelites.

5.3. Geodynamic implications for the transition between the Ottawa and the Rigolet orogenic phases

Our results also provide clues about the temporal evolution of a large, hot, long-duration orogen. First, the discordant nature of the studied PDG (Fig. 4a, d, g, Turlin et al., 2017) suggests that rocks of the Allochthonous Belt, after their proposed Ottawa flow (Indares et al., 2000; Rivers, 2008) were behaving as a passive lid to the flowing partially molten rocks of the underlying Parautochthonous Belt (Jannin et al., 2018b) during the Rigolet phase of the Grenvillian Orogeny. Evidence that it was still relatively hot at ca. 1005-1000 Ma (Indares and Dunning, 2018; Turlin et al., 2018) further suggests that this passive panel had not reached the upper crust, but was still in the middle crust, acting as a transfer zone for felsic magma. Furthermore, the (i) age range of the PDGs, the (ii) trace element contents (U, Yb, Y) of their zircon grains, and (iii) their Lu-Hf-O isotope signatures imply that partial melting of metapelites from the Parautochthonous Belt was underway by ca. 1005-1000 Ma underneath the study area (Fig. 11a). This age is the same as *HP* partial melting documented in metapelites of this belt cropping out along the shore of the Manicouagan Reservoir ca. 80 km to the north, along the azimuth of their stretching lineation (Jannin et al., 2018a). Inasmuch as northward-directed flow within a low-viscosity channel was documented for these rocks (Fig. 11b, Jannin et al., 2018b), it is very likely that our results imply that a channel at least 80 km long existed at that time.

Conclusions

Zircon grains from monazite- and allanite-bearing pegmatitic granite dykes (PGDs) hosted in the Allochthonous Belt of the central Grenville Province exhibit the geochemical character of continental igneous granitoids and lack textural, chemical and U-Pb isotopic evidence for inheritance. Therefore, they represent reliable witnesses of magmatic and post-magmatic processes.

The U-Pb zircon ages of ca. 1005-1000 Ma confirm that intrusion of monazite- and allanite-bearing PGDs occurred at the transition between the previously defined Ottawa and Rigolet tectonic-metamorphic phases of the Grenvillian Orogeny. Taken together, their (i) trace element signatures typical of continental granitoids, (ii) lower sub-chondritic ϵ_{Hf_t} values than plutonic rocks of the Allochthonous Belt, (iii) Hf model ages between 2.05 and 2.44 Ga, and (iv) supra-mantle dominated $\delta^{18}\text{O}_{\text{V-SMOW}}$ values point to the derivation of the PGDs by the partial melting of Paleoproterozoic-Archean metasedimentary rocks from the Parautochthonous Belt represented in this area by the Knob Lake Group metapelites.

The results of this study provide the first evidence (i) that LREE-rich peraluminous pegmatitic granite dykes can be derived by partial melting of metasedimentary rocks. Furthermore, they show that (ii) metasedimentary units from the Parautochthonous Belt were partially molten beneath the cooled Allochthonous Belt at the transition between the Ottawa and the Rigolet orogenic phases at ca. 1005 Ma during progressive horizontal flow of the partially molten root of the Grenville orogenic belt.

Acknowledgements

The authors would like to thank the Ministère de l'Énergie et des Ressources naturelles (Québec, Canada) for providing technical and financial support for the field work and analyses. This contribution constitutes a Ministère de l'Énergie et des Ressources naturelles du Québec

(Canada) publication no. 8449 - 2017-2018 - 04. The authors are grateful to Pierre-Arthur Groulier (Memorial University, NL, Canada) for his help during field work, to Robert Joussemet, Frédéric Diot, Jean-Marie Fischbach, and Christophe Gauthier (Steval, GeoRessources, Nancy) for their help in sample preparation and separation. The authors also thank Bernard Bingen and Trond Slagstad for their constructive review, and Guochun Zhao for editorial handling. This work was funded by the Labex Ressources 21 (supported by the French National Research Agency – France) through the national program “Investissements d’avenir”, reference ANR-10-LABX-21–LABEX RESSOURCES 21 and the Région Grand-Est. It benefited from the framework of the DIVEX “Rare earth element” research program.

References

- Augland, L.E., Moukhsil, A., Solgadi, F., Indares, A., McFarlane, C., 2015. Pinwarian to Grenvillian magmatic evolution in the central Grenville Province: new constraints from ID-TIMS U-Pb ages and coupled Lu-Hf S-MC-ICP-MS data. *Canadian Journal of Earth Sciences* 52, 701–721. doi:10.1139/cjes-2014-0232
- Ayres, L.D., Černý, P., 1982. Metallogeny of granitoid rocks in the Canadian Shield. *Can. Mineral.* 20, 439–536.
- Barbarin, B., 1999. A review of the relationships between granitoid types, their origins and their geodynamic environments. *Lithos* 46, 605–626. doi:10.1016/S0024-4937(98)00085-1
- Bea, F., 1996. Residence of REE, Y, Th and U in Granites and Crustal Protoliths; Implications for the Chemistry of Crustal Melts. *J. Petrology* 37, 521–552. doi:10.1093/petrology/37.3.521
- Belousova, E.A., Kostitsyn, Y.A., Griffin, W.L., Begg, G.C., O'Reilly, S.Y., Pearson, N.J., 2010. The growth of the continental crust: Constraints from zircon Hf-isotope data. *Lithos* 119, 457–466. doi:10.1016/j.lithos.2010.07.024
- Carr, S.D., Easton, R.M., Jamieson, R.A., Culshaw, N.G., 2000. Geologic transect across the Grenville orogen of Ontario and New York. *Can. J. Earth Sci.* 37, 193–216. doi:10.1139/e99-074
- Cawood, P.A., Hawkesworth, C.J., Dhuime, B., 2013. The continental record and the generation of continental crust. *GSA Bulletin* 125, 14–32. doi:10.1130/B30722.1
- Černý, P., Ercit, T.S., 2005. The classification of granitic pegmatites revisited. *Can. Mineral.* 43, Part 6, 2005–2026.

- Černý, P., London, D., Novák, M., 2012. Granitic Pegmatites as Reflections of Their Sources. *Elements* 8, 289–294. doi:10.2113/gselements.8.4.289
- Chappell, B.W., White, A.J.R., 2001. Two contrasting granite types: 25 years later. *Australian Journal of Earth Sciences* 48.
- Corfu, F., Hanchar, J.M., Hoskin, P.W.O., Kinny, P., 2003. Atlas of Zircon Textures. *Reviews in Mineralogy and Geochemistry* 53, 469–500. doi:10.2113/0530469
- Corrigan, L., van Breemen, O., 1997. U - Pb age constraints for the lithotectonic evolution of the Grenville Province along the Mauricie transect, Quebec. *Can. J. Earth Sci.* 34, 299–316. doi: 10.1139/e17-027
- Crowley, J.L., Brown, R.L., Gervais, F., Gibson, H.D., 2008. Assessing Inheritance of Zircon and Monazite in Granitic Rocks from the Monashee Complex, Canadian Cordillera. *J. Petrology* 49, 1915–1929. doi:10.1093/petrology/egn047
- David, J., 2006. Géochronologie d'échantillons provenant de Géologie Québec, année 2005-2006 - Rapport final. Ministère de l'Énergie et des Ressources Naturelles, Québec GM 63236, 12 p.
- David, J., Moukhsil, A., Clark, T., Hébert, C., Nantel, S., Dion, C., Sappin, A.-A., 2009. Datations U-Pb effectuées dans les provinces de Grenville et de Churchill en 2006-2007. Ministère des Ressources naturelles et de la Faune, Québec, RP2009-03, 32 p.
- de Sigoyer, J., Vanderhaeghe, O., Duchêne, S., Billerot, A., 2014. Generation and emplacement of Triassic granitoids within the Songpan Ganze accretionary-orogenic wedge in a context of slab retreat accommodated by tear faulting, Eastern Tibetan plateau, China. *Journal of Asian Earth Sciences*, 88, 192–216. doi: 10.1016/j.jseas.2014.01.010

- Dhuime, B., Hawkesworth, C.J., Cawood, P.A., Storey, C.D., 2012. A Change in the Geodynamics of Continental Growth 3 Billion Years Ago. *Science* 335, 1334–1336. doi:10.1126/science.1216066
- Dunning, G., Indares, A., 2010. New insights on the 1.7–1.0 Ga crustal evolution of the central Grenville Province from the Manicouagan – Baie Comeau transect. *Precambrian Research* 180, 204–226. doi:10.1016/j.precamres.2010.04.005
- Eglinger, A., Thébaud, N., Zeh, A., Davis, J., Miller, J., Parra-Avila, L.A., Loucks, R., McCuaig, C., Belousova, E., 2017. New insights into the crustal growth of the Paleoproterozoic margin of the Archean Kéména-Man domain, West African craton (Guinea): Implications for gold mineral system. *Precambrian Research* 292, 258–289. doi:10.1016/j.precamres.2016.11.012
- Ercit, T.S., 2005. REE-enriched granitic pegmatites. *Short Course Notes - Geological Association of Canada* 17, 175–199.
- Farina, F., Stevens, G., Gerdes, A., Frei, D., 2014. Small-scale Hf isotopic variability in the Peninsula pluton (South Africa): the processes that control inheritance of source Hf/Hf diversity in S-type granites. *Contrib. Mineral. Petrol.* 168, 1–18. doi:10.1007/s00410-014-1065-8
- Ferry, J.M., Watson, E.B., 2007. New thermodynamic models and revised calibrations for the Ti-in-zircon and Zr-in-rutile thermometers. *Contrib. Mineral. Petrol.* 154, 429–437. doi:10.1007/s00410-007-0201-0
- Fowler, A.D., Doig, R., 1983. The age and origin of Grenville Province uraniferous granites and pegmatites. *Can. J. Earth Sci.* 20, 92–104. doi:10.1139/e83-009

- Geisler, T., Schaltegger, U., Tomaschek, F., 2007. Re-equilibration of Zircon in Aqueous Fluids and Melts. *Elements* 3, 43–50. doi:10.2113/gselements.3.1.43
- Geisler, T., Ulonska, M., Schleicher, H., Pidgeon, R.T., Bronswijk, W. van, 2001. Leaching and differential recrystallization of metamict zircon under experimental hydrothermal conditions. *Contrib Mineral Petrol* 141, 53–65. doi:10.1007/s004100000202
- Gerdes, A., Zeh, A., 2009. Zircon formation versus zircon alteration — New insights from combined U–Pb and Lu–Hf in-situ LA-ICP-MS analyses, and consequences for the interpretation of Archean zircon from the Central Zone of the Limpopo Belt. *Chemical Geology, Accessory minerals as tracers of crustal processes* 261, 230–243. doi:10.1016/j.chemgeo.2008.03.005
- Gerdes, A., Zeh, A., 2006. Combined U–Pb and Hf isotope LA-(MC-)ICP-MS analyses of detrital zircons: Comparison with SHRIMP and new constraints for the provenance and age of an Armorican metasediment in Central Germany. *Earth and Planetary Science Letters* 249, 47–61. doi:10.1016/j.epsl.2006.06.039
- Gobeil, A., Hébert, C., Clark, T., Beaumier, M., Perreault, S., 2002. Géologie de la région du lac De la Blache (22K/03 et 22K/04). Ministère des Ressources Naturelles, Québec, RG 2002-01, 53 p.
- Grimes, C.B., John, B.E., Kelemen, P.B., Mazdab, F.K., Wooden, J.L., Cheadle, M.J., Hanghøj, K., Schwartz, J.J., 2007. Trace element chemistry of zircons from oceanic crust: A method for distinguishing detrital zircon provenance. *Geology* 35, 643–646. doi:10.1130/G23603A.1
- Groulier, P.-A., Indares, A., Dunning, G., Moukhsil, A., Jenner, G., 2018a. Syn-orogenic magmatism over 100 m.y. in high crustal levels of the central Grenville Province:

- Characteristics, age and tectonic significance. *Lithos* 312–313, 128–152. doi: 10.1016/j.lithos.2018.04.025
- Groulier, P.-A., Indares, A., Dunning, G., Moukhsil, A., Wälle, M., 2018b. Peri-Laurentian, Pinwarian-age oceanic arc crust preserved in the Grenville Province: Insights from the Escoumins supracrustal belt. *Precambrian Research* 311, 37–64. doi: 10.1016/j.precamres.2018.04.001.
- Hanchar, J.M., Finch, R.J., Hoskin, P.W.O., Watson, E.B., Cherniak, D.J., Mariano, A.N., 2001. Rare earth elements in synthetic zircon: Part 1. Synthesis, and rare earth element and phosphorus doping. *American Mineralogist* 86, 667–680. doi:10.2138/am-2001-5-607
- Hawkesworth, C., Cawood, P., Kemp, T., Storey, C., Dhuime, B., 2009. A Matter of Preservation. *Science* 323, 49–50. doi:10.1126/science.1168549
- Hayden, L.A., Watson, E.B., 2007. Rutile saturation in hydrous siliceous melts and its bearing on Ti-thermometry of quartz and zircon. *Earth and Planetary Science Letters* 258, 561–568. doi:10.1016/j.epsl.2007.04.020
- Hoffman, P.F., 1989. Precambrian geology and tectonic history of North America The geology of North America. *Geol. Soc. Am. : Boulder, CO, United States, United States*, pp. 447–512.
- Hoskin, P.W.O., Schaltegger, U., 2003. The Composition of Zircon and Igneous and Metamorphic Petrogenesis, in: Hanchar, J.M., Hoskins, P.W.O. (Eds.), *Zircon., Reviews in Mineralogy and Geochemistry*, Vol. 53. Mineralogical Society of America, pp. 27–62.

- Hynes, A., Indares, A., Rivers, T., Gobeil, A., 2000. Lithoprobe line 55: integration of out-of-plane seismic results with surface structure, metamorphism, and geochronology, and the tectonic evolution of the eastern Grenville Province. *Can. J. Earth Sci.* 37, 341–358. doi:10.1139/e99-076
- Hynes, A., Rivers, T., 2010. Protracted continental collision — evidence from the Grenville Orogen. *Can. J. Earth Sci.* 47, 591–620. doi:10.1139/E10-003
- Indares, A., Dunning, G., 2018. Metamorphic Evolution of the central Grenville Province (Manicouagan area): a review. In: Government of Quebec Report MM2017-01, ed: A. Moukhsil, 20 p.
- Indares, A., Dunning, G., 2001. Partial Melting of High-P–T Metapelites from the Tshenukutish Terrane (Grenville Province): Petrography and U–Pb Geochronology. *J. Petrology* 42, 1547–1565. doi:10.1093/petrology/42.8.1547
- Indares, A., White, R.W., Powell, R., 2008. Phase equilibria modelling of kyanite-bearing anatectic paragneisses from the central Grenville Province. *Journal of Metamorphic Geology* 26, 815–836. doi:0.1111/j.1525-1314.2008.00788.x
- Indares, A., Dunning, G., Cox, R., Gale, D., Connelly, J., 1998. High-pressure, high-temperature rocks from the base of thick continental crust: Geology and age constraints from the Manicouagan Imbricate Zone, eastern Grenville Province. *Tectonics* 17, 426–440. doi:10.1029/98TC00373
- Jannin, S., Gervais, F., Moukhsil, A., Augland, L.E., Crowley, J.L., 2018a. Déformations tardigrenvilliennes dans la Ceinture parautochtone (Province de Grenville centrale): contraintes géochronologiques par couplage de méthodes U/Pb de haute résolution spatiale et de haute précision. *Can. J. Earth Sci.* 55(4), 406-435. doi: 0.1139/cjes-2017-0129

- Jannin, S., Gervais, F., Moukhsil, A., Augland, L.E., 2018b. Late-Grenvillian channel flow in the central Grenville Province (Manicouagan Reservoir area): New constraints from a structural and geochronological study of the Allochthon Boundary Thrust. *Journal of Structural Geology* 115, 132–151. doi: 10.1016/j.jsg.2018.07.019
- Jordan, S.L., Indares, A., Dunning, G., 2006. Partial melting of metapelites in the Gagnon terrane below the high-pressure belt in the Manicouagan area (Grenville Province): pressure–temperature (P–T) and U–Pb age constraints and implications. *Can. J. Earth Sci.* 43, 1309–1329. doi:10.1139/E06-038
- Ketchum, J.W.F., Jamieson, R.A., Heaman, L.M., Culshaw, N.G., Krogh, T.E., 1994. 1.45 Ga granulites in the southwestern Grenville province: Geologic setting, P-T conditions, and U-Pb geochronology. *Geology* 22, 215–218. doi:10.1130/0091-7613(1994)022<0215:GGITSG>2.3.CO;2
- King, E.M., Valley, J.W., Davis, D.W., Edwards, G.R., 1998. Oxygen isotope ratios of Archean plutonic zircons from granite–greenstone belts of the Superior Province: indicator of magmatic source. *Precambrian Research* 92, 365–387. doi:10.1016/S0301-9268(98)00082-5
- Krogh, T.E., 1994. Precise U-Pb ages for Grenvillian and pre-Grenvillian thrusting of Proterozoic and Archean metamorphic assemblages in the Grenville Front tectonic zone, Canada. *Tectonics* 13, 963–982. doi:10.1029/94TC00801
- Lasalle, S., Dunning, G., Indares, A., 2014. In situ LA–ICP–MS dating of monazite from aluminous gneisses: insights on the tectono-metamorphic history of a granulite-facies domain in the central Grenville Province. *Can. J. Earth Sci.* 51, 558–572. doi:10.1139/cjes-2013-0170

- Lasalle, S., Fisher, C.M., Indares, A., Dunning, G., 2013. Contrasting types of Grenvillian granulite facies aluminous gneisses: Insights on protoliths and metamorphic events from zircon morphologies and ages. *Precambrian Research* 228, 117–130. doi:10.1016/j.precamres.2013.01.014
- Lasalle, S., Indares, A., 2014. Anatectic record and contrasting P-T paths of aluminous gneisses from the central Grenville Province. *Journal of Metamorphic Geology* 32, 627–646. doi:10.1111/jmg.12083
- Lentz, D.R., 1991. Petrogenesis of uranium-, thorium-, molybdenum-, and rare earth element-bearing pegmatites, skarns, and veins in the central metasedimentary belt of the Grenville Province, Ontario and Quebec. (Unpublished Ph.D. thesis). University of Ottawa (Canada).
- London, D., 2016. Rare-Element Granitic Pegmatites. *Reviews in Economic Geology* 18, 165–193.
- Maity, B., Indares, I., 2018. The Geon 14 arc-related mafic rocks from the central Grenville Province. *Can. J. Earth Sci.* 55, 545–570. doi:10.1139/cjes-2017-0197
- Martin, L., Duchêne, S., Deloule, E., Vanderhaeghe, O., 2008. Mobility of trace element and oxygen in zircon during metamorphism: Consequences for geochemical tracing. *Earth and Planetary Science Letters* 267, 161–174. doi:10.1016/j.epsl.2007.11.029
- Martin, L., Duchêne, S., Deloule, E., Vanderhaeghe, O., 2006. The isotopic composition of zircon and garnet: a record of the metamorphic history of Naxos, Greece. Special Volume “Geochronology of Metamorphism, Deformation and Metallogenesis”. *Lithos* 87, 174–192. doi: 10.1016/j.lithos.2005.06.016

- Martin, R.F., De Vito, C., 2005. The Patterns of Enrichment in Felsic Pegmatites Ultimately Depend on Tectonic Setting. *Can. Mineral.* 43, 2027–2048. doi:10.2113/gscanmin.43.6.2027
- Masson, S.L., Gordon, J.B., 1981. Radioactive mineral deposits of the Pembroke-Renfrew area (No. 23), Mineral Deposits Circ. Ont. Geol. Surv.
- McDonough, W.F., Sun, S. -s., 1995. The composition of the Earth. *Chemical Geology, Chemical Evolution of the Mantle* 120, 223–253. doi:10.1016/0009-2541(94)00140-4
- Moukhsil, A., Solgadi, F., 2018a. Géologie et potentiel minéral et cadre géodynamique des roches de la région du réservoir Daniel-Johnson (Manicouagan), partie centrale de la Province de Grenville. Abdelali Moukhsil coordonnateur. Ministère de l'Énergie et des Ressources naturelles, Québec. MM2017-01, 4–92.
- Moukhsil, A., Solgadi, F., 2018b. La Province de Grenville au Québec : une province à orogénies et évènements multiples. *Bulletin de la société géologique de France, Géologues* no 198, 17–20.
- Moukhsil, A., Solgadi, F., Belkacim, S., Elbasbas, A., Augland, L.E., 2014. Géologie de la région du lac Okaopéo, Côte-Nord. Ministère de l'Énergie et des Ressources Naturelles, Québec, RG 2014-03, 34 p.
- Moukhsil, A., Solgadi, F., Clark, T., Blouin, S., Indares, A., Davis, D.W., 2013a. Géologie du nord-ouest de la région du barrage Daniel-Johnson (Manic 5), Côte-Nord. Ministère des Ressources Naturelles, Québec, RG 2013-01, 46 p.
- Moukhsil, A., Solgadi, F., Indares, A., Belkacim, S., 2013b. Géologie de la région septentrionale du réservoir aux Outardes 4, Côte-Nord. Ministère des Ressources Naturelles, Québec, RG 2013-03, 33 p.

- Moukhsil, A., Solgadi, F., Lacoste, P., Gagnon, M., David, J., 2012. Géologie de la région du lac du Milieu (SNRC 22O03, 22O04, 22O06, 22J13 et 22J14). Ministère des Ressources Naturelles et de la Faune, Québec, RG 2012-01, 33 p.
- Moukhsil, A., Lacoste, P., Simard, M., Perreault, S., 2007. Géologie de la région septentrionale de Baie-Comeau (22F07, 22F08, 22F09, 22F15 et 22F16). Ministère des Ressources naturelles et de la Faune, Québec, RP 2007-04, 16 p.
- Moukhsil, A., Lacoste, P., Gobeil, A., David, J., 2009. Synthèse géologique de la région de Baie-Comeau. Ministère des Ressources naturelles et de la Faune, Québec, RG 2009-03, 30 p.
- Moyen, J.-F., Laurent, O., Chelle-Michou, C., Couzinié, S., Vanderhaeghe, O., Zeh, A., Villaros, A., Gardien, V., 2017. Collision vs. subduction-related magmatism: Two contrasting ways of granite formation and implications for crustal growth. *Lithos, Eighth Hutton Symposium on Granites and Related Rocks* 277, 154–177. doi:10.1016/j.lithos.2016.09.018
- Müller, A., Ihlen, P.M., Snook, B., Larsen, R., Flem, B., Bingen, B., and Williamson, B.J., 2015. The chemistry of quartz in granitic pegmatites of southern Norway: petrogenetic and economic implications. *Economic Geology* 110, 1737–1757. doi:10.2113/econgeo.110.7.1737
- Pearce, J.A., Harris, N.B.W., Tindle, A.G., 1984. Trace Element Discrimination Diagrams for the Tectonic Interpretation of Granitic Rocks. *Journal of Petrology* 25(4), 956–983.
- Pidgeon, R.T., 1992. Recrystallisation of oscillatory zoned zircon: some geochronological and petrological implications. *Contrib Mineral Petrol* 110, 463–472. doi:10.1007/BF00344081

- Pidgeon R.T., Nemchin A.A. and Cliff, J., 2013. Interaction of weathering solutions with oxygen and U-Pb isotopic systems of radiation damaged zircon from an Archean granite, Darling Range Batholith, Western Australia. *Contrib. Mineral. Petrol.* 166, 511-523.
- Rayner, N., Stern, R.A., Carr, S.D., 2005. Grain-scale variations in trace element composition of fluid-altered zircon, Acasta Gneiss Complex, northwestern Canada. *Contrib Mineral Petrol* 148, 721–734. doi:10.1007/s00410-004-0633-8
- Rivers, T., 2012. Upper-crustal orogenic lid and mid-crustal core complexes: signature of a collapsed orogenic plateau in the hinterland of the Grenville Province. *Can. J. Earth Sci.* 49, 1–42. doi:10.1139/e11-014
- Rivers, T., 2009. The Grenville Province as a large hot long-duration collisional orogen – insights from the spatial and thermal evolution of its orogenic fronts. Geological Society, London, Special Publications 327, 405–444. doi:10.1144/SP327.17
- Rivers, T., 2008. Assembly and preservation of lower, mid, and upper orogenic crust in the Grenville Province—Implications for the evolution of large hot long-duration orogens. *Precambrian Research* 167, 237–259. doi:10.1016/j.precamres.2008.08.005
- Rivers, T., 1997. Lithotectonic elements of the Grenville Province: review and tectonic implications. *Precambrian Research* 86, 117–154. doi:10.1016/S0301-9268(97)00038-7
- Rivers, T., 1980. Revised stratigraphic nomenclature for Aphebian and other rock units, southern Labrador Trough, Grenville Province. *Can. J. Earth Sci.* 17, 668–670. doi:10.1139/e80-062

- Rivers, T., Corrigan, D., 2000. Convergent margin on southeastern Laurentia during the Mesoproterozoic: tectonic implications. *Can. J. Earth Sci.* 37, 359–383. doi: 10.1139/e99-067
- Rivers, T., Culshaw, N., Hynes, A., Indares, A., Jamieson, R., Martignole, J., 2012. The Grenville Orogen - A Post-LITHOPROBE Perspective, in: *Tectonic Styles in Canada: The LITHOPROBE Perspective*, Geological Association of Canada, Special Paper 49. J.A. Percival, F.A. Cook, and R.M. Clowes, pp. 97–236.
- Rivers, T., Ketchum, J., Indares, A., Hynes, A., 2002. The High Pressure belt in the Grenville Province: architecture, timing, and exhumation. *Can. J. Earth Sci.* 39, 867–893.
- Rivers, T., Martignole, J., Gower, C.F., Davidson, A., 1989. New tectonic divisions of the Grenville Province, Southeast Canadian Shield. *Tectonics* 8, 63–84. doi:10.1029/TC008i001p00063
- Roback, R.C., 1996. Characterization and tectonic evolution of a Mesoproterozoic island arc in the southern Grenville Orogen, Llano uplift, central Texas. *Tectonophysics* 265, 29–52. doi: 10.1016/S0040-1951(96)00145-X
- Rubatto, D., 2017. Zircon: The Metamorphic Mineral. *Reviews in Mineralogy & Geochemistry* 83, 261–295. doi:10.2138/rmg.2017.83.09
- Sappin, A.-A., Constantin, M., Clark, T., van Breemen, O., 2009. Geochemistry, geochronology, and geodynamic setting of Ni–Cu ± PGE mineral prospects hosted by mafic and ultramafic intrusions in the Portneuf–Mauricie Domain, Grenville Province, Quebec. *Can. J. Earth Sci.* 46, 331–353. doi: 10.1139/E09-022

- Seydoux-Guillaume, A.M., Bingen, B., Paquette, J.L., Bosse, V., 2015. Nanoscale evidence for uranium mobility in zircon and the discordance of U–Pb chronometers. *Earth and Planetary Science Letters* 409, 43–48. doi: 10.1016/j.epsl.2014.10.044
- Slagstad, T., Hamilton, M.A., Jamieson, R.A. and Culshaw, N.G., 2004. Timing and duration of melting in the mid orogenic crust: Constraints from U–Pb (SHRIMP) data, Muskoka and Shawanaga domains, Grenville Province, Ontario. *Canadian Journal of Earth Sciences* 41, 1339–1365. doi: 10.1139/e04-068
- Spencer, C.J., Cawood, P.A., Hawkesworth, C.J., Prave, A.R., Roberts, N.M.W., Horstwood, M.S.A., Whitehouse, M.J., 2015. Focus paper: Generation and preservation of continental crust in the Grenville Orogeny. *Geoscience Frontiers* 6, 357–372. doi:10.1016/j.gsf.2014.12.001
- Tang, M., Wang, X.-L., Shua, X.-J., Wang, D., Yanga, T., Goponc, P., 2014. Hafnium isotopic heterogeneity in zircons from granitic rocks: Geochemical evaluation and modeling of “zircon effect” in crustal anatexis. *Earth and Planetary Science* 389, 188–199. doi: 10.1016/j.epsl.2013.12.036
- Timmermann, H., Jamieson, R.A., Parrish, R.R., Culshaw, N.G., 2002. Coeval migmatites and granulites, Muskoka domain, southwestern Grenville Province, Ontario. *Can. J. Earth Sci.* 39, 239–258. doi:0.1139/E01-076
- Toé, W., Vanderhaeghe, O., André-Mayer, A.-S., Feybesse, J.-L., Milési, J.-P., 2013. From migmatites to granites in the Pan-African Damara orogenic belt, Namibia. *Journal of African Earth Sciences* 85, 62–74. doi:10.1016/j.jafrearsci.2013.04.009

- Tucker, R.D., Gower, C.F., 1994. A U-Pb geochronological framework for the Pinware Terrane, Grenville Province, Southeast Labrador. *Journal of Geology* 102, 67.
- Turlin, F., André-Mayer, A.-S., Moukhsil, A., Vanderhaeghe, O., Gervais, F., Solgadi, F., Groulier, P.-A., Poujol, M., 2017. Unusual LREE-rich, peraluminous, monazite- or allanite-bearing pegmatitic granite in the central Grenville Province, Québec. *Ore Geology Reviews* 89, 627–667. doi:10.1016/j.oregeorev.2017.04.019
- Turlin, F., Deruy, C., Eglinger, A., Vanderhaeghe, O., André-Mayer, A.-S., Poujol, M., Moukhsil, A., Solgadi, F., 2018. A 70 Ma record of suprasolidus conditions in the large, hot, long-duration Grenville Orogen. *Terra Nova* 30-3, 233-243. doi: 10.1111/ter.12330.
- Valley, J.W., 2003. Oxygen Isotopes in Zircon. *Reviews in Mineralogy and Geochemistry* 53, 343–385. doi:10.2113/0530343
- Valley, J.W., Lackey, J.S., Cavosie, A.J., Clechenko, C.C., Spicuzza, M.J., Basei, M.A.S., Bindeman, I.N., Ferreira, V.P., Sial, A.N., King, E.M., Peck, W.H., Sinha, A.K., Wei, C.S., 2005. 4.4 billion years of crustal maturation: oxygen isotope ratios of magmatic zircon. *Contrib. Mineral. Petrol.* 150, 561–580. doi:10.1007/s00410-005-0025-8
- van Gool, J.A.M., Rivers, T., Calon, T., 2008. Grenville Front zone, Gagnon terrane, southwestern Labrador: Configuration of a midcrustal foreland fold-thrust belt. *Tectonics* 27, TC1004. doi:10.1029/2006TC002095
- Van Kranendonk, M.J.V., Kirkland, C.L., 2013. Orogenic climax of Earth: The 1.2–1.1 Ga Grenvillian superevent. *Geology* 41, 735–738. doi:10.1130/G34243.1
- Villaros, A., Buick, I.S., Stevens, G., 2012. Isotopic variations in S-type granites: an inheritance from a heterogeneous source? *Contrib. Mineral. Petrol.* 163, 243–257. doi:10.1007/s00410-011-0673-9

- Watson, E.B., Harrison, T.M., 1983. Zircon saturation revisited—temperature and composition effects in a variety of crustal magma types. *Earth Planet. Sci. Lett.* 64, 295–304.
- Watt, G.R., Burns, I.M., Graham, G.A., 1996. Chemical characteristics of migmatites: accessory phase distribution and evidence for fast melt segregation rates. *Contrib Mineral Petrol* 125, 100–111
- Zeh, A., Gerdes, A., 2012. U–Pb and Hf isotope record of detrital zircons from gold-bearing sediments of the Pietersburg Greenstone Belt (South Africa)—Is there a common provenance with the Witwatersrand Basin? *Precambrian Research* 204, 46–56. doi:10.1016/j.precamres.2012.02.013
- Zeh, A., Stern, R.A., Gerdes, A., 2014. The oldest zircons of Africa—Their U–Pb–Hf–O isotope and trace element systematics, and implications for Hadean to Archean crust–mantle evolution. *Precambrian Research* 241, 203–230. doi:10.1016/j.precamres.2013.11.006

Figure captions

Figure 1: a: Map of Proterozoic Laurentia showing the different north-American orogens with Paleozoic and younger cover omitted (modified from Hoffman, 1989; Rivers et al., 2012). The northern dashed line represents the boundary between Internal and External Paleoproterozoic Laurentia and the southern dashed line represents the Grenville Front (GF); b: Simplified geological map of the Grenville Province. Extension of supracrustal sequences in the foreland after Rivers (2008). Abbreviations: 1 = Grenville Province, light grey represents the inferred extension of subsurface allochthonous Grenville Province; 2 = Granite-Rhyolite Igneous Province, ca. 1.50-1.34 Ga and reworked equivalents in the Grenville Province; 3 = Mid-Continental Rift system; 4 = Paleoproterozoic orogens, ca. 1.9-1.8 Ga, ca. 1.65 Ga and reworked equivalents in the Grenville Province; 5 = cratons; Cn = Canyon domain; G = Gagnon Terrane; GF = Grenville Front; HJ = Hart-Jaune terrane; HSG = Huron Supergroup; KLG = Knob Lake Group; L = Lelukuau terrane; MG = Mistassini Group; OG = Otish Group; SLG = Seal Lake Group; Ts = Tshenukutish terrane.

Figure 2: Geological map of the central Grenville Province (Quebec) showing the position of the investigated monazite- and allanite-bearing pegmatitic granite dykes and of the cross-section presented in Fig. 11 (modified after Moukhsil et al., 2014; Turlin et al., 2017). Abbreviations: ABT = Allochthon Boundary Thrust; Aln-bearing PGD = allanite-bearing pegmatitic granite dyke; MIZ = Manicouagan Imbricate Zone; Mnz-bearing PGD = monazite-bearing pegmatitic granite dyke.

Figure 3: Simplified geological map of the environment of the investigated REE-rich pegmatitic granite dykes in the Lac Okaopéo region (modified after Moukhsil et al., 2014; Turlin et al., 2017). Orange and grey diamonds represent monazite-bearing and allanite-bearing pegmatitic granite outcrops respectively. ¹: Augland et al. (2015); ²: Gobeil et al. (2002); ³:

David (2006); ⁴: Dunning and Indares (2010); ⁵: David et al. (2009); ⁶: Moukhsil et al. (2013a); ⁷: Moukhsil et al. (2012); ⁸: Lasalle et al. (2013).

Figure 4: Representative photographs of outcrops, facies and petrography of monazite- and allanite-bearing pegmatitic granite dykes from the central Grenville Province investigated in this study. a: photograph of a discordant contact of a monazite-bearing dyke intruding paragneisses from the Plus-Value Complex. Note the Stockscheider texture underlining the contact in the dyke; b: typical quartz+feldspar+biotite dominated intermediate facies of the 13-AM-13 monazite-bearing PGD as presented by Turlin et al. (2017) sampled for this study; c: early- to syn-monazite crystallization zircon crystal (SEM) from the 13-AM-13 monazite-bearing dyke; d: photograph of a typical allanite-bearing pegmatitic granite dyke from the 13-TC-5072 outcrop showing discordant contacts with its host (metamonzogranite from the Bardoux Plutonic Suite); e: typical quartz+feldspar+biotite assemblage completed with phenocrysts of allanite from the 13-TC-5072 allanite-bearing pegmatitic granite dyke; f: sub-euhedral zircon grains and its relationships with the quartz+plagioclase+K-feldspar+biotite±allanite assemblage; g: photograph of a discordant contact of an allanite-bearing dyke with its host from the 13-FS-1202 outcrop (quartz-metamonzodiorite from the Castoréum Plutonic Suite). Note the textural continuity between the PGD and ‘apparently boudinaged’ granitic veins transposed in the foliation of the host; h: typical facies observed in the 13-FS-1202 pegmatitic granite; i: prismatic zircon grains and their relationships with the quartz+plagioclase+K-feldspar+biotite±allanite assemblage. Abbreviations: Aln = allanite; Bt = biotite; Fsp = feldspar; Mnz = monazite; Pl = plagioclase; Qtz = quartz; Ser = sericite; Zrc = zircon.

Figure 5: Back scattered electron (BSE) images of zircon grains from the 13-AM-13 monazite-bearing and the 13-TC-5072 and 13-FS-1202 allanite-bearing pegmatitic granite dykes of the central Grenville Province. The circles mark the position of the laser ablation analyses for trace

element (orange), and of the SIMS spots for $\delta^{18}\text{O}$ analyses (blue), with associated Ca+Fe and ΣLREE content and $\delta^{18}\text{O}_{\text{V-SMOW}}$ signatures. *Italic trace element values identify the LREE-Ca-Fe-rich domains (see text for details).* a: zircon grains from the monazite-bearing dyke (sample 13-AM-13); b and c: zircon grains from the allanite-bearing dykes (samples 13-TC-5072 and 13-FS-1202).

Figure 6: Back scattered electron (BSE) images of zircon grains from the 13-AM-13 monazite-bearing and the 13-TC-5072 and 13-FS-1202 allanite-bearing pegmatitic granite dykes of the central Grenville Province. The circles mark the position of the laser ablation analyses for U-Pb dating (red) and Lu-Hf isotopes (green), with associated $^{207}\text{Pb}/^{206}\text{Pb}$ ages and $\epsilon\text{Hf}_{(1003\text{ Ma})}$ signatures. a: zircon grains from the monazite-bearing dyke (sample 13-AM-13); b and c: zircon grains from the allanite-bearing dykes (samples 13-TC-5072 and 13-FS-1202).

Figure 7: Trace element characteristics of zircon grains from the monazite- and the allanite-bearing pegmatitic granite dykes investigated in this study. a: ΣLREE (ppm) vs Ca+Fe (ppm) diagram. The grey shaded area represents the pristine domain defined on the basis of the LREE, Ca and Fe contents (see text for details). Note that a majority of zircon analyses are restricted to the pristine domain and that the analyses from the monazite- and the allanite-bearing dykes display distinct trends of enrichments, the former being more sensible to a LREE increase and associated with an increase of the Th/U ratio; b: Th/U vs ΣLREE (ppm) diagram. Note the distinct trends of increasing LREE content, associated with an increase of the Th/U ratio for zircon from the monazite-bearing pegmatitic granite dyke and with rather stable Th/U ratio for the others; c: $\text{Sm}_{\text{N}}/\text{La}_{\text{N}}$ vs Ca+Fe (ppm) diagram of zircon grains showing the correlation between the increase in the Ca and Fe contents and the flattening of the LREE slope; d: Ti-in-zircon temperature vs Ca+Fe (ppm) diagram. The grey shaded area represents the pristine domain defined on the basis on the LREE, Ca and Fe contents (see text for details). Temperature

calculations are based on the thermometer defined by Ferry and Watson (2007). The computed temperatures of zircon from the monazite- and the 13-FS-1202 allanite-bearing dykes are correlated with an increase in the Ca and Fe contents. Therefore, only temperatures computed on zircon with a pristine character are considered as reliable; e: U/Yb vs Y (ppm) diagrams of Grimes et al. (2007). The grey shaded area represents the continental field defined by Grimes et al. (2007) (see text for details). Note that all analyses from both pristine and LREE-Ca-Fe-rich domains plot in the continental field; f to h: chondrite-normalized REE patterns of zircon grains (chondrite normalization after McDonough and Sun, 1995). The pristine zircon domains are associated with typical granitic zircon (see text for details). To the contrary, LREE-Ca-Fe-rich domains yield flat LREE patterns as shown by the loss of the Ce anomaly. The HREE patterns remain rather stable for both types.

Figure 8: $\delta^{18}\text{O}_{\text{V-SMOW}}$ signatures of zircon grains from the monazite- and the allanite-bearing pegmatitic granite dykes investigated in this study. a: probability density plot of $\delta^{18}\text{O}_{\text{V-SMOW}}$ signatures of zircon grains. Note the multimodal distribution of analyses from the 13-FS-1202 allanite-bearing PGD and the supra-mantle dominated distribution of other samples; b: Ca+Fe (ppm) vs $\delta^{18}\text{O}_{\text{V-SMOW}}$ signatures show no correlation between the Ca and Fe enrichments and the associated $\delta^{18}\text{O}_{\text{V-SMOW}}$ values. Abbreviation: ¹: Valley et al. (2005).

Figure 9: Concordia diagrams of U -Pb dating on magmatic zircon from the monazite-bearing pegmatitic granite dyke (13-AM-13) and from the allanite-bearing pegmatitic granite dykes (13-TC-5072 and 13-FS-1202) investigated in this study. Legend is similar to Figs. 7 and 8. a: Concordia plots of U-Pb data obtained on zircon from the monazite-bearing dyke (sample 13-AM-13, n = 48, data-point error ellipses are 2σ); b: Concordia plots of U-Pb data obtained on zircon from the 13-TC-5072 allanite-bearing dyke (n = 14, data-point error ellipses are 2σ); c: Concordia plots of U-Pb data obtained on zircon from the 13-FS-1202 allanite-bearing dyke (n

= 42, data-point error ellipses are 2σ); d and e: Ca+Fe (ppm) and Σ LREE (ppm) vs $^{207}\text{Pb}/^{206}\text{Pb}$ concordance for all three samples showing no correlations between non-pristine domains and the concordance of U-Pb dating analyses.

Figure 10: εHf_t signatures vs intrusion age of magmatic zircon from the monazite- and the 13-TC-5072 and 13-FS-1202 allanite-bearing pegmatitic granite dykes investigated in this study with reported values of allochthonous plutonic units from the Lac Okaopéo region (data from Augland et al., 2015). Note that the zircon grains from the monazite- and allanite-bearing pegmatitic granite dykes plot in a distinct crustal evolution domain than surrounding allochthonous plutonic units yielding to older T_{DM2} Hf model ages.

Figure 11: Schematic cross-section illustrating the geodynamic context of the petrogenesis of the monazite- and allanite-bearing pegmatitic granite dykes investigated in this study (modified after Turlin et al., 2018, integrating results from Jannin et al., 2018b). a: Petrogenesis of the monazite- and allanite-bearing PGDs and their link with the partial melting of the Parautochthonous Belt (this study); b: Evolution of the partially molten Grenvillian root towards lateral extrusion of the mid allochthonous and upper parautochthonous crusts associated with the Rigolet channel flow (integration of the investigated pegmatitic granite dyke in the results of Jannin et al., 2018b). Abbreviations: ABT/ABD = Allochthonous Boundary Thrust/Detachment; aHP = allochthonous high pressure Ottawaan crust; aM-LP = allochthonous mid to low pressure Ottawaan crust; Paraut. Crust = Parautochthonous crust; PGD = pegmatitic granite dyke; TSZ = Thachic shear zone.

Table 1: Summary of the results obtained on zircon grains from the monazite-bearing (13-AM-13) and two allanite-bearing (13-FS-1202 and 13-TC-5072) pegmatitic granite dykes from the central Grenville Province. Abbreviations: Aln-bearing PGD = allanite-bearing

pegmatitic granite dyke; Conc. = degree of concordance; Mnz-bearing PGD = monazite-bearing
pegmatitic granite dyke; Prist. = pristine; Temp. = temperature.

U m)	T h/U	Y b (ppm)	U/ Yb	Y (ppm)	Ce/ Ce* ^d	P r/ Pr* ^d	S m/ Sm* ^d	E u/ Eu* ^d	Sm N ^d / LaN ^d	Y b _{N^d} /Sm _{N^d}	Y b _{N^d} /Gd _{N^d}
37	0.	2	1.8	77	26.	0.	7.	0.	12		
8	36	08	2	7	36	12	12	06	90	56	14
51	0.	3	1.7	13	29.	0.	7.	0.	22		9.
8	60	02	2	24	02	11	87	06	68	37	4
49	0.	1	3.5	51	1.8	0.	4.	0.			9.
7	42	40	4	4	3	81	59	08	32	17	2
46	0.	2	1.7	10	21.	0.	7.	0.	13		
4	39	60	9	03	88	14	35	06	48	49	13
44	0.	2	2.0	84	27.	0.	7.	0.	13		
2	38	13	7	8	02	12	94	06	59	48	12
37	0.	8	4.5	28	36.	0.	7.	0.	51		
0	34	1	3	5	52	09	61	06	8	47	13
53	0.	2	1.7	12	36.	0.	8.	0.	18		
0	52	97	8	10	81	09	02	06	23	44	11
27	0.	1	2.3	45	32.	0.	7.	0.	44		
1	28	17	2	8	50	10	38	06	1	61	14
44	0.	2	2.0	78	20.	0.	8.	0.	12		
5	19	17	5	5	52	13	71	05	16	64	15
40	0.	1	2.0	72	18.	0.	7.	0.	10		
9	22	96	9	3	82	15	98	06	25	60	15
90	0.	2	4.2	10	1.1	1.	3.	0.		7.	5.
3	44	12	5	18	9	06	32	08	18	0	7
82	0.	2	3.9	90	1.2	1.	3.	0.			6.
1	45	07	7	0	5	02	42	08	18	10	7
60	0.	1	3.5	72	14.	0.	10	0.	86		
9	28	69	9	0	93	17	.02	04	1	42	10

67 5	0. 62	3 61	1.8 7	16 08	8.1 2	0. 27	6. 70	0. 08	12 5	23	7. 6
30 2 69 6	0. 28 0. 33	8 5 2 19	3.5 5 3.1 8	30 4 77 4	37. 49 21. 74	0. 08 0. 14	7. 62 8. 22	0. 06 0. 05	85 6 79 5	55 45	14 11
13 74	0. 60	3 69	3.7 2	16 36	21. 86	0. 13	7. 82	0. 06	15 58	23	6. 4
50 7	0. 37	1 38	3.6 8	51 5	29. 47	0. 11	7. 41	0. 06	10 08	47	12
70 7	0. 36	1 45	4.8 8	55 3	29. 46	0. 11	7. 83	0. 06	87 2	39	10
52 4	0. 43	2 44	2.1 5	10 40	1.4 7	0. 87	3. 21	0. 13	4.7	20	8. 9
62 8 41 7	0. 27 0. 32	2 17 1 88	2.8 9 2.2 2	10 09 75 7	3.3 9 30. 08	0. 56 0. 10	5. 20 8. 86	0. 08 0. 05	59 12 72	34 53	10 13
38 4	0. 34	1 00	3.8 3	32 5	28. 44	0. 11	7. 57	0. 06	34 4	54	15

49 6	0. 58	2 77	1.7 9	12 00	19. 06	0. 15	6. 98	0. 07	16 4	40	10
44 7	0. 37	2 26	1.9 7	80 5	18. 84	0. 15	7. 33	0. 06	21 8	52	13
44 0	0. 18	1 81	2.4 3	76 6	16. 93	0. 16	8. 87	0. 05	12 28	62	14
60 2	0. 66	3 25	1.8 5	14 87	3.9 9	0. 50	5. 85	0. 08		19	7. 1
34 9	0. 47	1 98	1.7 7	78 8	28. 92	0. 11	7. 34	0. 07	13 94	45	12
24 6	0. 16	8 6	2.8 6	33 2	13. 37	0. 21	7. 96	0. 05	33 6	63	15
34 9	1. 43	9 4	3.7 3	33 4	0.9 8	1. 07	3. 25	0. 16		4. 6	4. 9
42 8	0. 30	1 05	4.1 0	46 9	1.2 6	1. 01	2. 72	0. 17	16	16	8. 1
56 4	0. 39	1 69	3.3 3	56 6	14. 93	0. 19	7. 00	0. 07	22 0	39	11
75 6	0. 35	1 64	4.6 1	61 8	25. 85	0. 12	9. 19	0. 05	58 4	38	10
50 4	0. 39	1 09	4.6 4	40 2	35. 95	0. 09	7. 12	0. 07	79 2	44	12
81 9	0. 49	4 14	1.9 8	17 67	15. 26	0. 18	8. 76	0. 06	21 27	26	7. 5
49 3	0. 28	2 53	1.9 5	87 2	21. 93	0. 14	8. 48	0. 05	13 58	62	14
72 9	0. 33	1 97	3.6 9	76 6	26. 01	0. 12	9. 31	0. 05	93 8	38	10

60	0.	1	3.3	70	6.7	0.	8.	0.	16		
4	30	81	3	6	8	36	15	05	3	42	11
46	0.	1	3.2	58	16.	0.	9.	0.	94		
6	25	43	7	1	78	15	73	04	6	52	12

ACCEPTED MANUSCRIPT

56	0.	4	1.2	13	4.6	0.	5.	0.		11	
2	22	63	1	25	0	44	15	06	10	5	26
50	0.	4	1.2	12	2.8	0.	4.	0.		12	
6	21	02	6	35	5	56	10	08	3.8	2	27

38	0.	3	1.0	10	1.6	0.	2.	0.				
5	26	60	7	66	8	82	25	09	0.8	88	25	
55	0.	3	1.4	11	1.4	0.	1.	0.				
6	28	74	9	19	1	98	26	10	0.4	37	21	
47	0.	2	1.6	90	41.	0.	6.	0.		10		
9	24	92	4	9	18	06	86	07	90	9	24	
54	0.	4	1.2	12	71.	0.	6.	0.	97	14		
7	22	22	9	49	99	05	45	07	1	8	27	
66	0.	6	0.9	17	55.	0.	6.	0.	11	15		
8	25	72	9	74	36	06	48	07	00	4	27	
48	0.	3	1.2	12	5.8	0.	5.	0.		10		
9	23	90	5	12	8	37	58	07	18	3	23	
44	0.	3	1.2	10	3.3	0.	3.	0.				
5	22	66	1	44	9	57	98	08	6.6	90	25	
17	0.	1	1.2	38	38.	0.	5.	0.		20		
6	18	41	4	6	31	07	70	07	64	0	36	
54	0.	4	1.2	13	56.	0.	6.	0.	87	15		
0	22	44	1	04	74	06	51	07	8	8	28	
53	0.	4	1.1	13	60.	0.	6.	0.	98	15		
7	22	55	8	16	30	06	67	07	9	7	29	
89	0.	5	1.6	15	58.	0.	6.	0.	84	10		
7	27	38	7	93	90	06	60	07	5	9	23	
30	0.	2	1.4	48	154	0.	6.	0.	22	25		
1	18	07	5	7	.79	02	10	05	6	6	40	

77	0.	4	1.8	13	47.	0.	6.	0.	44		
7	28	23	3	14	64	07	92	07	2	87	20
46	0.	3	1.2	12	1.6	0.	2.	0.			
2	31	75	3	48	8	83	98	10	1.8	43	16
54	0.	3	1.5	10	9.4	0.	5.	0.			
7	27	49	7	04	9	24	46	08	18	96	23
48	0.	3	1.2	11	1.8	0.	3.	0.			
3	23	98	1	54	9	77	04	08	1.6	79	24
51	0.	4	1.1	12	6.0	0.	5.	0.		13	
4	21	31	9	33	0	35	08	07	14	6	28
48	0.	4	1.1	11	7.8	0.	5.	0.		14	
6	21	09	9	58	8	28	27	07	18	9	29
56	0.	5	1.1	15	38.	0.	6.	0.	32		
8	27	00	4	84	68	08	90	07	5	98	20
48	0.	3	1.2	11	55.	0.	6.	0.	87	15	
4	20	98	2	95	59	06	81	07	5	0	28
38	0.	3	1.1	98	10.	0.	5.	0.		11	
2	27	23	8	6	89	21	69	07	22	3	24
57	0.	3	1.5	11	11.	0.	5.	0.			
7	28	69	6	93	72	20	73	08	22	94	21
56	0.	3	1.6	10	4.4	0.	4.	0.			
1	27	35	7	39	8	42	68	08	6.0	87	21
55	0.	5	1.0	17	58.	0.	6.	0.	24		
0	34	04	9	59	05	06	93	07	10	89	17
41	0.	3	1.1	10	70.	0.	7.	0.	93	16	
4	18	56	6	10	74	05	02	07	8	4	31
46	0.	4	1.1	11	59.	0.	6.	0.	29	14	
4	25	03	5	38	25	05	66	07	7	9	28
34	0.	3	1.0	10	65.	0.	6.	0.	30	14	
5	26	42	1	08	36	05	27	07	4	8	27
49	0.	4	1.1	11	71.	0.	6.	0.	10	16	
8	21	36	4	61	74	05	29	07	72	2	30

47	0.	4	1.0	10	28.	0.	6.	0.		17	
6	22	47	6	91	67	09	10	07	80	2	31
48	0.	3	1.2	11	65.	0.	6.	0.	90	15	
9	20	93	4	73	42	05	91	07	0	4	29
54	0.	4	1.2	12	56.	0.	6.	0.	73	16	
5	20	26	8	67	17	06	22	07	9	2	28
37	0.	2	1.3	83	2.2	0.	3.	0.		10	
8	25	87	2	8	8	65	72	07	2.0	6	25
52	0.	4	1.1	13	4.1	0.	3.	0.		11	
8	22	71	2	24	7	47	27	13	7.3	9	27
70	0.	6	1.1	20	37.	0.	7.	0.	15		
5	33	04	7	37	18	08	20	07	26	71	16
31	0.	2	1.0	93	3.3	0.	3.	0.		10	
1	26	99	4	2	3	56	38	11	4.0	2	24
28	0.	2	1.0	62	101	0.	5.	0.	53	18	
0	21	57	9	4	.12	03	88	07	1	9	33
49	0.	4	1.2	12	1.7	0.	3.	0.			
1	25	03	2	87	3	81	28	07	1.6	86	22
67	0.	5	1.1	20	3.0	0.	5.	0.			
6	34	85	6	20	8	57	04	07	8.0	61	16
25	0.	2	1.1	65	103	0.	6.	0.	16	15	
5	23	32	0	9	.46	03	81	06	46	4	29
61	0.	5	1.2	14	52.	0.	6.	0.	50	14	
1	23	03	2	98	72	06	36	07	0	9	27
56	0.	3	1.4	12	45.	0.	6.	0.	36	10	
5	28	87	6	50	67	07	51	07	4	9	23
32	0.	2	1.4	82	21.	0.	7.	0.	13		
2	23	27	2	5	56	14	18	06	16	61	15
39	0.	2	1.4	10	17.	0.	7.	0.	12		
2	27	81	0	57	59	16	72	06	10	53	14
33	0.	2	1.3	89	21.	0.	7.	0.	14		
2	27	44	6	8	34	14	75	06	36	56	14
16	0.	1	1.5	37	35.	0.	7.	0.	69		
4	23	07	3	5	61	09	68	06	5	67	17
20	0.	7	2.8	16	214	0.	4.	0.	50	20	
6	07	1	9	5	.88	01	12	09	4	6	38

74	0.	3	2.1	13	1.2	0.	3.	0.				
1	32	49	2	75	8	93	82	10	4.1	27		11
40	0.	2	1.3	11	0.8	1.	3.	0.				
9	30	99	7	34	8	13	87	08	3.0	35		13
37	0.	2	1.4	10	2.9	0.	6.	0.				
1	32	64	1	81	2	51	22	07	15	31		10
30	0.	2	1.3	77	22.	0.	7.	0.	10			
5	23	20	8	4	03	14	65	06	13	65		16
46	0.	3	1.4	13	0.9	1.	0.	0.				
9	36	31	2	85	1	15	80	07	0.1	13		9.0
33	0.	2	1.3	85	2.2	0.	5.	0.				
1	24	46	4	7	0	58	83	06	3.9	62		16
46	0.	3	1.4	13	0.9	1.	3.	0.				
7	31	32	1	63	5	27	38	10	4.5	8		7.0
29	0.	2	1.3	76	8.9	0.	6.	0.				
1	23	15	5	2	1	20	27	07	26	65		16
39	0.	2	1.4	10	5.1	0.	7.	0.				
8	27	82	1	78	7	31	21	06	20	50		13
26	0.	1	1.3	69	1.6	0.	4.	0.				
7	24	98	4	7	3	76	70	07	3.8	48		15
43	0.	3	1.4	11	17.	0.	7.	0.				
2	27	09	0	49	93	16	52	06	10	56		14
43	0.	3	1.4	12	1.2	1.	3.	0.				
4	32	08	1	17	3	05	46	11	3.8	33		12
14	0.	7	1.8	21	57.	0.	4.	0.				
8	16	9	6	7	13	05	75	08	12	12		25
									9	4		

- ✓ Coeval monazite- and allanite-bearing peraluminous pegmatites (1005-1000 Ma)
- ✓ Intrusion in the Allochthonous Belt during the initiation of the Rigolet phase
- ✓ Partially molten Parautochthonous Belt below the Allochthonous Belt at ca. 1005 Ma
- ✓ LREE-rich pegmatites formed by partial melting of Paleoproterozoic-Archean metasediments

ACCEPTED MANUSCRIPT